

Involvement of GABAergic Interneuron Subtypes in 4-Aminopyridine-Induced Seizure-Like Events in Mouse Entorhinal Cortex *in Vitro*

 Paolo Scalmani,¹ Rosina Paterra,²  Massimo Mantegazza,^{3,4,5} Massimo Avoli,^{6,7} and Marco de Curtis¹

¹Epilepsy Unit and, ²Neuro-Oncology Unit, Fondazione IRCCS Istituto Neurologico Carlo Besta, Milano 20133, Italy, ³Université Côte d'Azur, 06560 Valbonne-Sophia Antipolis, France, ⁴Institute of Molecular and Cellular Pharmacology, Centre National de la Recherche Scientifique, Unité Mixte de Recherche 7275, Laboratoire d'Excellence/Canaux Ioniques d'Intérêt Thérapeutique, 06650 Valbonne-Sophia Antipolis, France, ⁵Institut National de la Santé et de la Recherche Médicale, 06650 Valbonne-Sophia Antipolis, France, ⁶Montreal Neurological Institute-Hospital, McGill University, Montreal, Quebec H3A 2B4, Canada, and ⁷Departments of Neurology and Neurosurgery and Physiology, McGill University, Montreal, Quebec H3A 2B4, Canada

Single-unit recordings performed in temporal lobe epilepsy patients and in models of temporal lobe seizures have shown that interneurons are active at focal seizure onset. We performed simultaneous patch-clamp and field potential recordings in entorhinal cortex slices of GAD65 and GAD67 C57BL/6J male mice that express green fluorescent protein in GABAergic neurons to analyze the activity of specific interneuron (IN) subpopulations during acute seizure-like events (SLEs) induced by 4-aminopyridine (4-AP; 100 μ M). IN subtypes were identified as parvalbuminergic (IN_{PV}, $n = 17$), cholecystokinergic (IN_{CCK}, $n = 13$), and somatostatinergic (IN_{SOM}, $n = 15$), according to neurophysiological features and single-cell digital PCR. IN_{PV} and IN_{CCK} discharged at the start of 4-AP-induced SLEs characterized by either low-voltage fast or hyper-synchronous onset pattern. In both SLE onset types, IN_{SOM} fired earliest before SLEs, followed by IN_{PV} and IN_{CCK} discharges. Pyramidal neurons became active with variable delays after SLE onset. Depolarizing block was observed in $\sim 50\%$ of cells in each INs subgroup, and it was longer in IN (~ 4 s) than in pyramidal neurons (< 1 s). As SLE evolved, all IN subtypes generated action potential bursts synchronous with the field potential events leading to SLE termination. High-frequency firing throughout the SLE occurred in one-third of IN_{PV} and IN_{SOM}. We conclude that entorhinal cortex INs are very active at the onset and during the progression of SLEs induced by 4-AP. These results support earlier *in vivo* and *in vivo* evidence and suggest that INs have a preferential role in focal seizure initiation and development.

Key words: epilepsy; *in vitro* slices; interneurons; patch clamp; seizures

Significance Statement

Focal seizures are believed to result from enhanced excitation. Nevertheless, we and others demonstrated that cortical GABAergic networks may initiate focal seizures. Here, we analyzed for the first time the role of different IN subtypes in seizures generated by 4-aminopyridine in the mouse entorhinal cortex slices. We found that in this *in vitro* focal seizure model, all IN types contribute to seizure initiation and that INs precede firing of principal cells. This evidence is in agreement with the active role of GABAergic networks in seizure generation.

Received June 17, 2022; revised Dec. 30, 2022; accepted Jan. 5, 2023.

Author contributions: M.A. and M.D.-C. designed research; P.S. and R.P. performed research; P.S., R.P., M.M., and M.D.-C. analyzed data; and P.S., M.A., and M.D.-C. wrote the paper.

This work was supported by Italian Ministry of Health Grants Current Research 2021 and RF 2018-12365681, Paolo Zorzi Association for Neuroscience Grant 2021-24 EPICARE Project, Canadian Institutes of Health Research Grants PJT153310, PJT166178 to M.A. and the French Agence National de la Recherche (ANR-11-LABX-0015-01 "LabEx ICST" and ANR-15-IDEX-01 "UCAJEDI") to Massimo Mantegazza. We thank Yuchio Yanagawa (Gunma University, Japan) for providing GAD67 knock-in mice and Gábor Szabó (Institute of Experimental Medicine, Budapest, Hungary) for providing GAD65 transgenic mice.

The authors declare no competing financial interests.

Correspondence should be addressed to Paolo Scalmani at paolo.scalmani@istituto-besta.it.

<https://doi.org/10.1523/JNEUROSCI.1190-22.2023>

Copyright © 2023 the authors

Introduction

Clinical and experimental studies have provided evidence for distinctive and region-specific network mechanisms associated with the onset of focal seizures (Perucca and O'Brien, 2015; Singh et al., 2015; Lagarde et al., 2016; Uva et al., 2017b; Devinsky et al., 2018; Di Giacomo et al., 2019; Gnatkovsky et al., 2019). Reproducible seizure patterns described in patients with temporal lobe epilepsy (TLE), have been replicated in *in vitro* preparations and in TLE animal models to identify network and cellular processes responsible for their generation and progression (Avoli et al., 2016; de Curtis and Avoli, 2016).

Two seizure onset patterns were observed in TLE patients during presurgical monitoring with intracranial EEG electrodes [low-voltage fast (LVF) and hypersynchronous (HYP); Engel, 1990]; these two onset patterns were confirmed in rodent TLE/hippocampal sclerosis models (Bragin et al., 1999; Riban et al., 2002; Grasse et al., 2013; Lévesque et al., 2013). Moreover, *in vitro* experiments performed in rodent brain slices (Lopantsev and Avoli, 1998a; Derchansky et al., 2008; Losi et al., 2010; Zhang et al., 2012; Lévesque et al., 2013; Behr et al., 2014; Avoli et al., 2016; Codadu et al., 2019) or in the isolated whole guinea pig brain (Uva et al., 2005; Boido et al., 2014a) confirmed the occurrence of LVF and HYP seizure onsets during application of convulsive drugs. Specifically, in entorhinal cortex slices that were perfused with a solution containing the potassium channel blocker 4-aminopyridine (4-AP), LVF seizures appeared to be associated with the activation of interneuronal networks (Lopantsev and Avoli, 1998a; Avoli et al., 2016). In the same *in vitro* model, HYP seizures were also shown to be accompanied by interneuron discharges (Derchansky et al., 2008) and prominent GABAergic postburst hyperpolarizations that progressively decrease in amplitude while unrestrained excitation is enhanced as seizure activity develops (Zhang et al., 2012; Avoli et al., 2016; Köhling et al., 2016).

Interestingly, *in vitro* experiments have shown that during 4-AP application, optogenetic activation of GABAergic interneurons (INs) induces SLEs with LVF-onset, whereas HYP seizure onset pattern occurred when principal cells were optogenetically stimulated; therefore, these data suggest that both types of seizure onset patterns can be generated under identical conditions by activating specific neuronal populations (Shiri et al., 2016). The involvement of entorhinal cortex (EC) interneurons in SLEs induced by 4-AP was confirmed by intracellular recordings performed on the guinea pig isolated brain (Gnatkovsky et al., 2008; Uva et al., 2015) and by single-unit recordings of putative INs in EC slices with tetrode wires (Lévesque et al., 2018). Interneuron activity, and the resulting GABA release, leads to massive activation of postsynaptic GABA_A receptors that favors seizure generation through intracellular accumulation of Cl⁻ and the subsequent increase in extracellular [K⁺] because of activation of the K⁺-Cl⁻ cotransporter-2 (Avoli et al., 1996a,b; Librizzi et al., 2017; Di Cristo et al., 2018). Moreover, optogenetic activation of parvalbumin (PV) and somatostatin (SOM) INs evokes epileptiform discharges similar to those occurring spontaneously during 4-AP application in cortical slices (Yekhlef et al., 2015; Shiri et al., 2016). Overall, these findings indicate that SLEs generated *in vitro* by cortical networks during 4-AP treatment are caused by enhanced interneuron activity. Therefore, in this study, we evaluated the participation of different subpopulations of GABAergic INs to the initiation and maintenance of SLEs induced by 4-AP in mouse EC slices.

Materials and Methods

Animal care and mouse lines. Experiments were conducted on C57BL/6J mice (Charles River Laboratories, <https://www.criver.com/products-services/find-model/jax-c57bl6j-mice?region=27>) according to European Directive 2010/63/UE, approved by institutional and national ethical committees (Protocol 711/2016-PR). All efforts were made to minimize the number of animals and their suffering. Mice were group housed (five per cage, or one male and two females per cage for breeding) on a 12 h light/dark cycle, with *ad libitum* water and food.

Entorhinal cortex brain slices. Brain slices were prepared as previously described (Mantegazza et al., 1998; Aracri et al., 2006) from 20–30-d-old C57BL/6J mice that selectively express the green fluorescent

protein (GFP) in GABAergic INs, specifically, GAD65-GFP transgenic male mice (López-Bendito et al., 2004) and GAD67-GFPΔneo knock-in mice (Tamamaki et al., 2003). GAD67 knock-in mice were provided by Y. Yanagawa (Gunma University, Japan), GAD65 transgenic mice were provided by G. Szabo (Institute of Experimental Medicine, Budapest, Hungary). Animals were decapitated under isoflurane anesthesia, the brain was quickly removed and placed in ice-cold modified ACSF (mACSF), which contained the following (in mM): 87 NaCl, 7 MgCl₂, 2.5 KCl, 0.5 CaCl₂, 21 NaHCO₃, 1.25 NaH₂PO₄, 25 glucose, and 75 sucrose. The mACSF was bubbled with 95% O₂/5% CO₂. Horizontal slices (400 μm thick) that contained the ventral hippocampus and the entorhinal cortex were cut with a vibratome (VT1200S, Leica) in ice-cold mACSF and were placed in an incubation chamber and bathed, at room temperature, in standard ACSF, which contained the following (in mM): 129 NaCl, 1 MgSO₄, 3 KCl, 1.6 CaCl₂, 21 NaHCO₃, 1.25 NaH₂PO₄, and 10 glucose.

Electrophysiological recordings. Electrophysiological recordings started after an incubation/recovery period of at least 1 h. One slice at the time was transferred to the recording chamber (Warner Instruments), and GFP-fluorescent INs were visualized by infrared video microscopy with a Nikon Eclipse FN1 microscope equipped with differential interference contrast (DIC) optics and a charge-coupled device camera (Hamamatsu). Simultaneous extracellular local field potential (LFP) and whole-cell, current-clamp patch-clamp (PC) recordings [Fig. 1A; LFP electrodes (LFPes) and PC electrodes (PCes)] were performed at 25°C with a MultiClamp 700B patch-clamp amplifier, a Digidata 1440a digitizer, and pClamp 10.2 software (Molecular Devices). Pipettes were pulled (Sutter Instruments) from borosilicate glass capillaries to a resistance of 2.5–3.0 MΩ (access resistance of 4–7 MΩ). The internal pipette solution for LFP recordings was mACSF, whereas for current-clamp patch-clamp recordings it contained the following (in mM): 120 K-gluconate, 15 KCl, 2 MgCl₂, 0.2 EGTA, 10 HEPES, 2 Na₂ATP, 0.2 Na₂GTP, 20 P-creatine, and RNase inhibitor (0.5 U/μl; catalog #AM2682, Invitrogen), pH 7.2, achieved with KOH.

For LFP recordings we used the MultiClamp 700B amplifier in *I* = 0 mode; for whole-cell recordings we used it in current-clamp mode maintaining, after appropriate bridge balance compensation, the cell resting membrane potential at −70 mV by injecting intracellular current. Whole-cell patch-clamp recordings were performed from the cell soma; INs were identified by GFP fluorescence (Fig. 1C, red arrow), pyramidal neurons (Pyr) were identified by their size and the pear-like appearance of the soma, and by the lack of GFP fluorescence (Fig. 1B, black arrow). Signals were filtered at 10 kHz and were sampled at 50 kHz. Signal analyses were performed using pClamp 10.5 and OriginPro 8.5 software (OriginLab).

Input/output (I/O) curves were obtained by injecting 2.5 s depolarizing current pulses that were increased by 10 pA steps (Fig. 2A,B). Action potential (AP) firing adaptation was measured quantifying interspike intervals between subsequent APs elicited by current pulses inducing depolarization ranging between 2 and 5 mV above AP firing threshold. In adapting neurons, the AP interval was short at the beginning of the depolarizing pulse-induced AP firing and long at its end. Neurons with unstable resting potential and/or variable firing patterns were discarded from the analysis.

Quantitative evaluation of AP dynamic changes was performed by phase plot analysis (Jenerick, 1963; Bean, 2007). The first derivative of the action potential (dV/dt measured as mV/ms; Fig. 2C, y-axis; Fig. 3A, dotted line) were plotted against the instantaneous membrane potential (measured in mV; Fig. 2C, x-axis; Fig. 3A, continuous line). AP features were represented as a loop in which the rising starting point represents the AP threshold ($V_{threshold}$; Fig. 3B), the extreme right value is the maximal voltage amplitude (V_{peak}), and the top and bottom peaks of the loop are the maximum rise slope (MRS), and the maximum decay slope (MDS), respectively. Phase plot loops were smoothed with an Origin SP line function. Phase plot analysis magnifies and highlights $V_{threshold}$, V_{peak} , MRS, and MDS changes (Fig. 3B, arrows). Mean phase plots (Fig. 2C) were constructed by aligning the AP peak (Fig. 3A, continuous line) to the first derivative peak (black dotted line) for each cell; the obtained curves were further aligned by placing the peaks of the APs at the zero y point of the first derivative as shown in Figure 3A (red dotted line); average errors were reported on phase plot x-axis (membrane potential) and

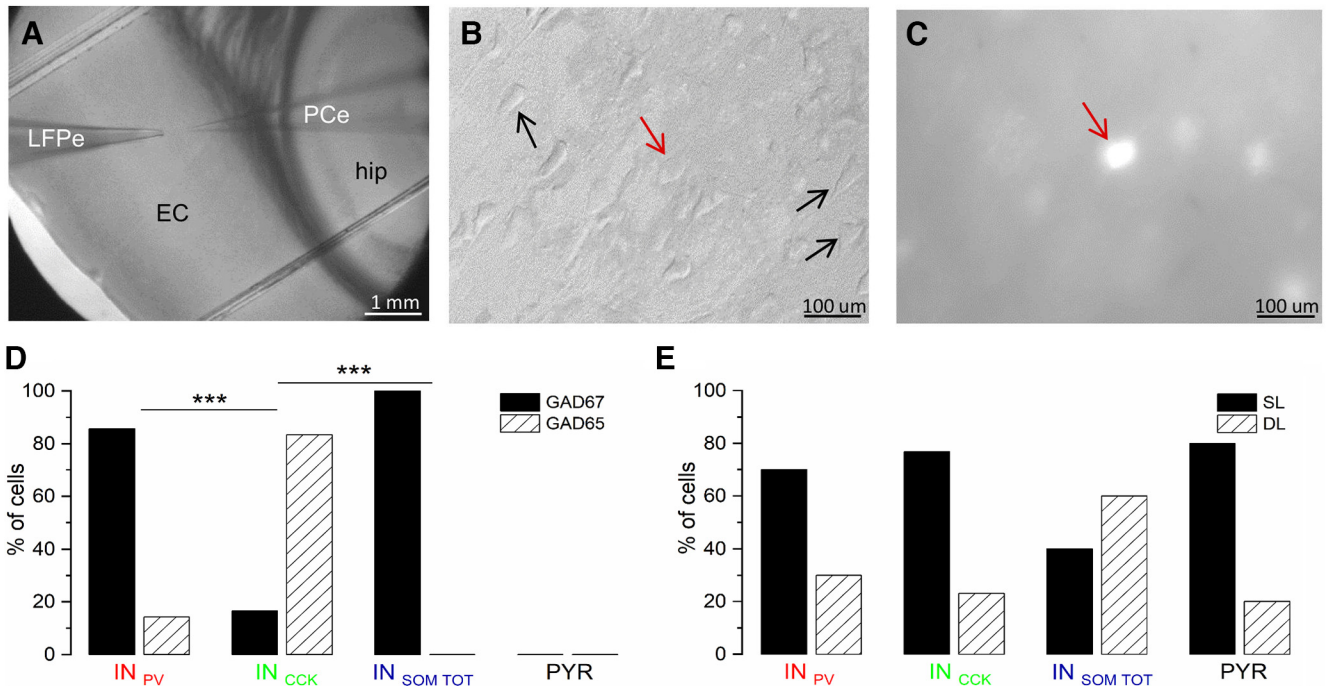


Figure 1. Experimental setup. **A**, Microphotograph of a horizontal hippocampal/entorhinal mouse slice ($10\times$ magnification). Recording LFPe and PCe are illustrated. hip, Hippocampal formation. **B**, **C**, High-magnification images have been obtained with infrared DIC (**B**) and fluorescence microscopy (**C**). GFP-containing INs (red arrow) in an EC slice from GAD65 and GAD67 mouse and GFP-negative neurons (black arrows) with typical pyramidal soma. **D**, Percentage of IN subtypes recorded in EC slices obtained from GAD65 (IN_{PV} = 14.3%, IN_{CCK} = 83.3%, IN_{SOM} = 0%, PYRs = 0%, striped columns) and GAD67 mice (IN_{PV} = 85.7%, IN_{CCK} = 16.7%, IN_{SOM} = 100%, PYRs = 0%, black columns). **E**, Percentage of IN subtypes and PYRs recorded from superficial EC layers 2–3 (IN_{PV} = 70%, IN_{CCK} = 77%, IN_{SOM} = 40%, PYRs = 80%, black columns) and deep EC layers 4 and 5 (IN_{PV} = 30%, IN_{CCK} = 23%, IN_{SOM} = 60%, PYRs = 20%, striped columns). For statistical analysis, Fisher's exact test with Bonferroni's correction was used (* = $p < 0.05$, ** = $p < 0.01$, *** = $p < 0.001$).

y -axis (slope) in Fig. 2C. The graphs in Figure 3B were constructed on average curves aligned to the AP peak. SLEs were induced perfusing brain slices with freshly made ACSF with low Mg^{2+} (0.5 mM) and 100 μ M 4-AP (catalog #A78403, Sigma-Aldrich).

Single-cell reverse transcription and digital PCR. For single-cell digital PCR (sc-dPCR), a gentle negative pressure was applied to the patch pipette after completing the electrophysiological recording to harvest the cell cytoplasm containing RNA. The intracellular material pulled in the electrode (5 μ l) was placed in a test tube (catalog #AB-0620, Thermo Fisher Scientific) for short treatment with DNAase and then for reverse transcription (RT) using the SuperScript IV VILO Master Mix with ezDNase enzyme (catalog #11766050, Thermo Fisher Scientific). The RNA from each individual cell was subjected to gDNA digestion at 37°C for 2 min in a total volume of 10 μ l (gDNA digestion reaction mix, 1 μ l ezDNase enzyme, 1 μ l ezDNase Buffer RNA to 10 μ l in RNase-free H₂O), it was briefly centrifuged and placed on ice and then reverse transcribed in a total volume of 20 μ l (4 μ l Super Script IV VILO Master Mix, 6 μ l nuclease-free water, 10 μ l gDNA digested RNA). RT was conducted with subsequent cycles at 25°C for 10 min, at 50°C for 10 min, and at 85°C for 5 min. The material was finally stored at -80°C until preamplification.

Digital PCR was conducted after cDNA preamplification in a 30 μ l TaqMan PreAmp Master Mix (catalog #4384267, Thermo Fisher Scientific), 15 μ l Pooled TaqMan Gene Expression Assays (0.2 \times), and 15 μ l cDNA. For the assay pool, an equal volume of each 20 \times TaqMan Gene expression Assay was combined (Thermo Fisher Scientific; Table 1) at a final concentration of 0.4 \times per assay. PreAmp cycling protocol was the following: 10 min enzyme activation at 95°C followed by 10 denaturation cycles at 95°C for 15 s and annealing at 60°C for 4 min followed by 10 min at 99°C for enzyme inactivation and hold at 4°C. In each preamplification session a No Template Control was always inserted, and the same was then used as a negative control in the dPCR. After preamplification, sc-dPCR was conducted in a Quant Studio 3D Digital PCR System (Thermo Fisher Scientific), detection channels Fluorescein (FAM)/Sybr Green, VIC, and ROX. Both target and reference genes were run in duplex; each dPCR chip was loaded with 16 μ l

reaction mix containing 6 μ l preamplified PCR mixture, 8 μ l Master Mix (Quant Studio 3D Master Mix V2, Thermo Fisher Scientific), 0.8 μ l endogenous control assay (*Gapdh_VIC* 20 \times), 0.8 μ l target gene assay (*Pv/Cck/Som*), and 0.4 μ l nuclease-free water. For each cell, five chips were loaded, one for each target. The dPCR chips were loaded into a ProFlex PCR System (Thermo Fisher Scientific) for 10 min at 96°C, 2 min at 60°C, and 30 s at 98°C for 45 cycles, then 2 min at 60°C and hold at 10°C. The chips were read on QuantStudio 3D Digital PCR System, and data were processed with Quant Studio 3D Analysis Suite (Thermo Fisher Scientific). For each cell, the statistical analysis (Fig. 4A–C) was obtained by equaling the sum of the copies/ μ l of each target at 100 and the individual targets as a percentage of the total.

Statistics. Statistical analysis was performed using Prism 6.0 software (GraphPad) or Origin 2021 (OriginLab). The Fisher exact test with Bonferroni's correction was used for the data expressed as a percentage (Fig. 1D,E); ANOVA one-way tests with Tukey's *post hoc* test were used for normally distributed data, and the Kruskal–Wallis test with Dunn's *post hoc* test to determine pairwise differences between groups were used for data not normally distributed. A *t* test and Mann–Whitney tests were used for single population data distributed either normally or not, respectively (Fig. 7). The Wilcoxon test was used to test the location of a population based on a sample of data. Comparisons of actual and expected frequencies for categorical data were obtained with the chi-square goodness-of-fit test.

Results

Our study was based on simultaneous LFP and intracellular patch-clamp recordings that were performed from 45 INs and 10 PYRs in 55 horizontal EC slices; 33 and 22 cells were recorded from superficial and deep EC layers, respectively (Fig. 1E). In seven additional EC slices, the effects of neurotransmitter receptor antagonists were analyzed during extracellular LFP recordings (see below).

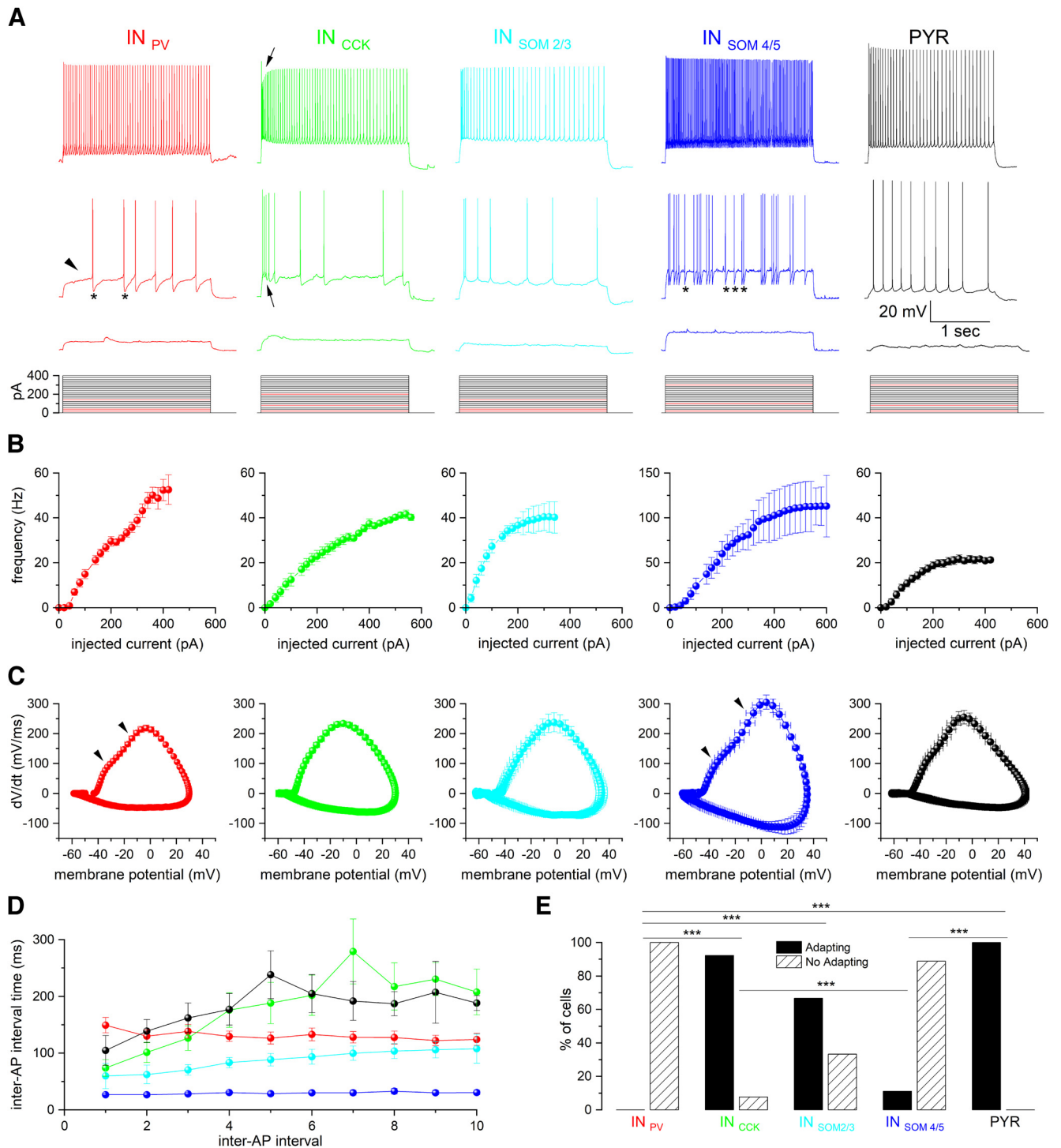


Figure 2. Different types of interneurons identified by firing properties. INs recorded in EC slices with typical features of IN_{PV} (red traces/plots), IN_{CCK} (green), IN_{SOM} (blue), and typical PYR (black) neurons are illustrated; different firing properties were observed in IN_{SOM} recorded either in superficial (2/3) or deep (4/5) EC layers (light blue and dark blue, respectively). **A**, Representative traces of AP firing recorded from INs and PYRs in GAD-67/65 mouse EC slices, elicited by intracellular injection of a 2.5 s depolarizing pulse (bottom row); the three traces illustrate responses evoked by current pulses just below (bottom) and just above AP threshold (middle) and by large current pulses (top row). Asterisks mark post-AHP in IN_{PV} and $IN_{SOM4/5}$; the arrowhead points to the delayed AP firing at threshold depolarization typically observed in IN_{PV} ; arrows mark AP bursting at threshold, typical of IN_{CCK} (see below, Results). **B**, Average firing rates of INs and PYRs constructed from I/O plots that display the AP frequency in response to intracellular depolarizing current pulses of increasing amplitude. The curves describe the average data (mean \pm SD) obtained from 17 IN_{PV} , 11 IN_{CCK} , 6 $IN_{SOM2/3}$, 9 $IN_{SOM4/5}$, and 10 PYRs. **C**, Average AP phase plots showing the first derivative of membrane potential changes as a function of instantaneous AP membrane potential (dV/dt vs mV) for the different types of INs and PYRs. APs are represented as a loop in which the starting point is the threshold membrane potential, and the extreme right point is the maximal AP voltage amplitude. The average of 16 IN_{PV} , 11 IN_{CCK} , 5 $IN_{SOM2/3}$, 9 $IN_{SOM4/5}$, and 10 PYRs. The arrowheads (left and right) indicate the two AP accelerations typically observed in IN_{PV} and $IN_{SOM4/5}$. **D**, Average interspike intervals of the first 11 APs evoked by intracellular depolarizing current injection just above firing threshold in IN_{PV} (red, $n = 16$), IN_{CCK} (green, $n = 12$), $IN_{SOM2/3}$ (light blue, $n = 5$), $IN_{SOM4/5}$ (blue, $n = 8$), and PYRs (black, $n = 10$). **E**, Percentage of adapting (black column) and nonadapting (striped column) neurons divided per IN subtypes and PYRs. Adapting neurons, $IN_{PV} = 0\%$, $IN_{CCK} = 92.3\%$, $IN_{SOM2/3} = 66.6\%$, $IN_{SOM4/5} = 11.1\%$, and PYRs = 100%. Nonadapting neurons, $IN_{PV} = 100\%$, $IN_{CCK} = 7.7\%$, $IN_{SOM2/3} = 33.4\%$, $IN_{SOM4/5} = 88.9\%$, and PYRs = 0%. For statistical analysis, Fisher's exact test with Bonferroni's correction was used (* = $p < 0.05$, ** = $p < 0.01$, *** = $p < 0.001$).

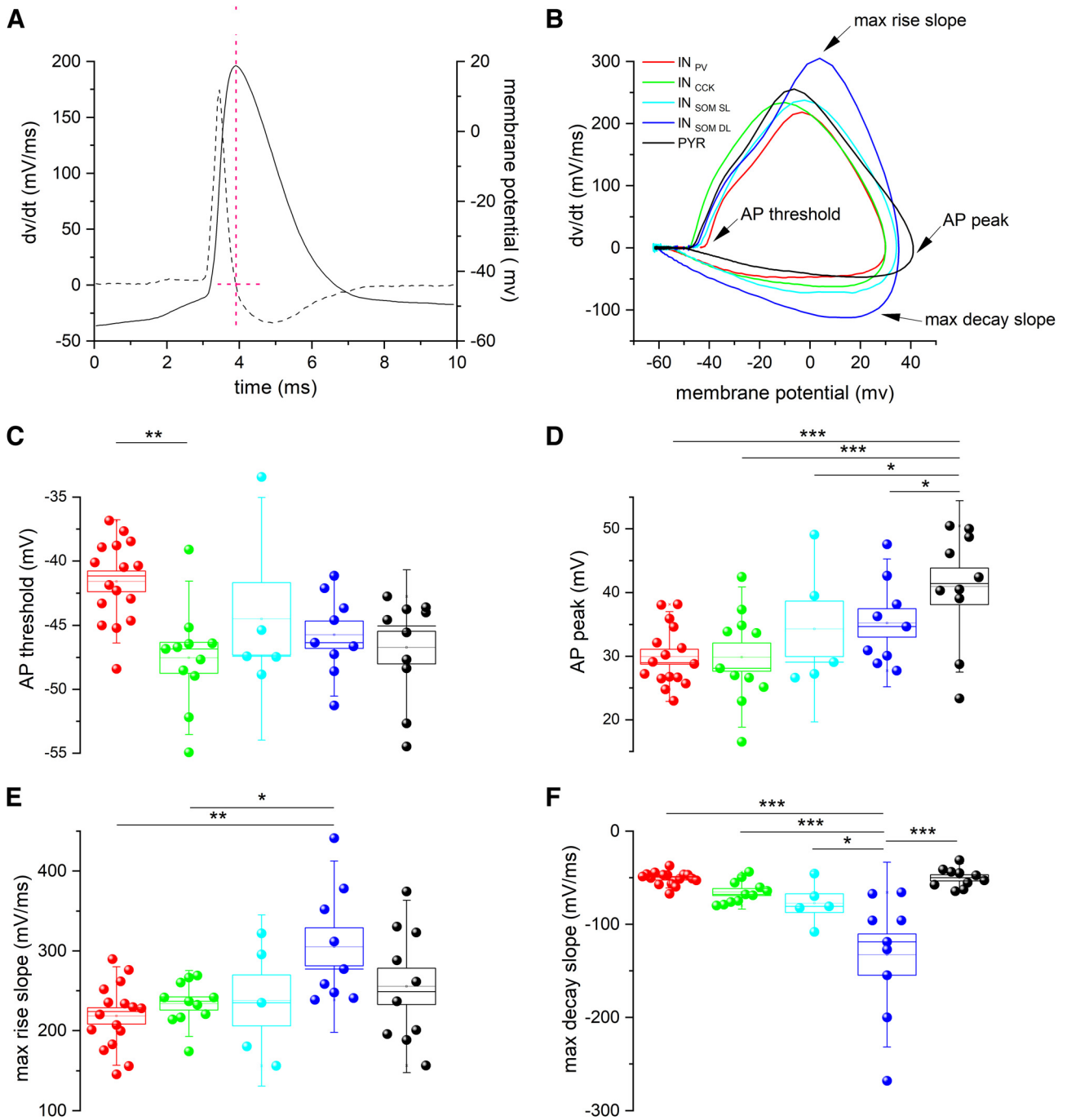


Figure 3. Main features of APs recorded from the different subtypes of INs and PYRs. **A, B**, Representative trace of AP (continuous line) and its first derivative (dashed line) used to construct AP phase plots. The y-axis refers to the AP (right) and the first derivative (left), respectively; the pink dotted line indicates the alignment used to create the phase plots shown in **B**. AP phase plots of the different subtypes of EC neurons (**B**). **C–F**, The arrows indicate the parameters analyzed. **C**, AP threshold quantification (in mV), $IN_{PV} = -41.57 \pm 0.80$, $IN_{CCK} = -47.54 \pm 1.20$, $IN_{SOM2/3} = -44.50 \pm 2.82$, $IN_{SOM4/5} = -45.73 \pm 1.06$, $PYRs = -46.73 \pm 1.27$. **D**, AP peak amplitude quantification (in mV), $IN_{PV} = 29.93 \pm 1.17$, $IN_{CCK} = 29.86 \pm 2.21$, $IN_{SOM2/3} = 34.30 \pm 4.36$, $IN_{SOM4/5} = 35.21 \pm 2.23$, $PYRs = 40.97 \pm 2.83$. **E**, Max rise slope quantification (mV/ms), $IN_{PV} = 218.40 \pm 10.26$, $IN_{CCK} = 233.97 \pm 8.28$, $IN_{SOM2/3} = 237.88 \pm 31.96$, $IN_{SOM4/5} = 305.20 \pm 23.82$, $PYRs = 255.55 \pm 22.76$. **F**, Maximum decay slope quantification (mV/ms), $IN_{PV} = -50.61 \pm 1.75$, $IN_{CCK} = -65.37 \pm 3.6$, $IN_{SOM2/3} = -77.33 \pm 10.16$, $IN_{SOM4/5} = -132.56 \pm 22.06$, $PYRs = -50.09 \pm 3.28$. IN_{PV} (red dots, $n = 16$), IN_{CCK} (green dots, $n = 11$), $IN_{SOM2/3}$ (light blue dots, $n = 5$), $IN_{SOM4/5}$ (blue dots, $n = 9$) and $PYRs$ (black dots, $n = 10$). ANOVA with Tukey's *post hoc* test and Kruskal–Wallis test with Dunn's *post hoc* test were used (* = $p < 0.05$, ** = $p < 0.01$, *** = $p < 0.001$).

Interneuron subtypes

Based on both firing and AP properties, we grouped INs in four subtypes (Fig. 2A–C). We identified 17 presumed parvalbuminergic INs (IN_{PV} ; red traces and symbols throughout); these cells generated APs that were followed by pronounced after-hyperpolarizing potentials (AHPs; Fig. 2A, left, asterisks; Kecskés et al., 2020; Fernandez et al., 2022). IN_{PV} sustained high-frequency AP

firing up to 60 Hz and demonstrated a linear average current/voltage relationship (Fig. 2B, I/O plots) with no frequency rate adaptation just above firing threshold (Fig. 2D, red dots). Moreover, as reported in previous studies (Goldberg et al., 2008; Helm et al., 2013; Miyamae et al., 2017) all IN_{PV} showed a delay in the AP onset following injections of current just above AP threshold (Fig. 2A, arrowheads). Phase plot analysis demonstrated

Table 1. Digital PCR assay details

Gene symbol	Assay ID	Reference Sequence	Probe Exon Location	Amplicon size	Probe dye
Cck	Mm00446170_m1	NM_031161.4	Probe spans exons 2–3	79	FAM
Pv	Mm00443100_m1	NM_013645.3	Probe spans exons 1–2	77	FAM
Som	Mm00436671_m1	NM_009215.1	Probe spans exons 1–2	86	FAM
Gapdh	Mm99999915_g1	NM_008084.3	Probe spans exons 2–3	109	VIC

FAM is a fluorescent dye with an absorption wavelength of 495 nm and an emission wavelength of 517 nm modified *Aequorea victoria* fluorescein; VIC is a fluorescent compound with an excitation peak at 526 nm and an emission peak at 543 nm.

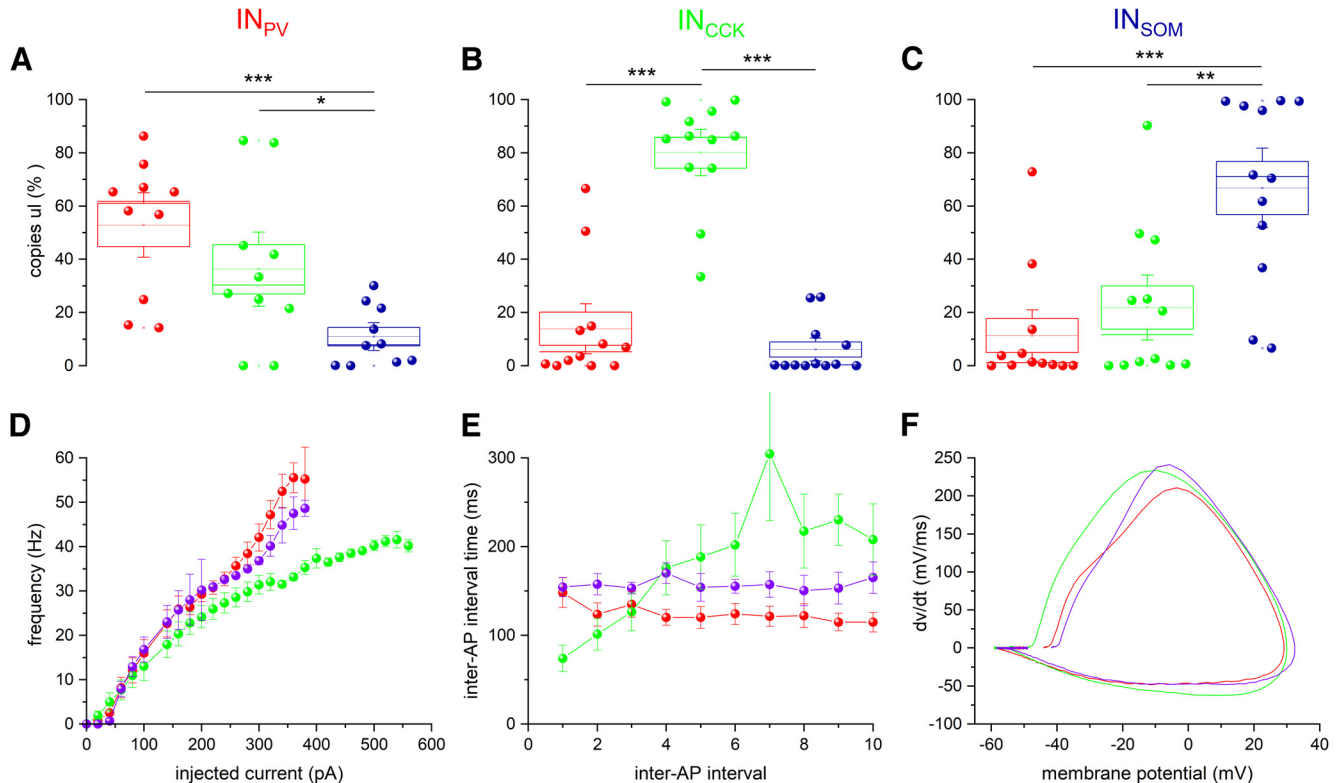


Figure 4. Single-cell digital PCR analysis of IN subgroups and electrophysiological features of IN_{PV} with elevated CCK cDNA content. **A–C**, Top, Expression of *Pv* (red), *Cck* (green), and *Som* (blue) cDNA in 11, 12, and 12 INs, respectively, defined as IN_{PV} (**A**), IN_{CCK} (**B**), and IN_{SOM} (**C**) based on electrophysiological properties. The result, expressed as copies/ μ l, were normalized assuming that the total copies/ μ l of all targets (*PV* + *CCK* + *SOM*) is equal to 100 (percentage); the percentage of each target was calculated as the relative ratio. For statistical analysis and data distribution, ANOVA with Tukey's *post hoc* test was used; for data not normally distributed, Kruskal–Wallis test with Dunn's *post hoc* test was used (* = $p < 0.05$, ** = $p < 0.01$, *** = $p < 0.001$). Bottom, Data obtained in IN_{PV} that expressed CCK at levels higher than *PV* are illustrated by purple dots and lines ($n = 4$); red symbols mark data from the remaining IN_{PV} group ($n = 13$); green symbols identify IN_{CCK} data ($n = 13$). **D**, Average firing rate (I/O plot) of INs in response to intracellular current pulses of increasing amplitude; **E**, Average interval between the first 11 APs evoked by intracellular depolarizing current injection just over the threshold. **F**, Averaged AP phase plots showing the derivative of membrane potential (dv/dt vs mV) as a function of instantaneous membrane potential during action potential for the different groups of INs. The data confirm that the four IN_{PV} with high CCK content showed electrophysiological features different from IN_{CCK} .

two accelerations in the AP rising phase (Fig. 2C, arrowheads; Fig. 3B). IN_{PV} showed a higher AP threshold compared with INs cholecystikinin (IN_{CCK} ; Fig. 3C) and a lower MRS than $IN_{SOM4/5}$ and PYRs (Fig. 3E). In all putative IN_{PV} in which sc-dPCR was performed (11 of 17 IN_{PV} identified by intrinsic electrophysiological properties) the presence of cDNA for *PV* was confirmed (Fig. 4A, red dots). Interestingly, a subpopulation of IN_{PV} cells also coexpressed CCK (Fig. 4A, green dots) and SOM (Fig. 4A, dark blue dots; see below, Discussion). Firing and AP properties were not different in IN_{PV} recorded in superficial or deep EC layers.

Presumed cholecystikinergic INs (Fig. 2A–D IN_{CCK} ; $n = 13$; green traces and graphs) responded with a burst of APs to threshold firing depolarization (Fig. 2A, arrows in green trace, second row). As previously reported (Varga et al., 2010; Armstrong et al., 2016), the IN_{CCK} I/O relationship showed a lower rate of maximum discharge (~ 40 Hz) during depolarizing pulse injections

than IN_{PV} . Most IN_{CCK} (92.3%) showed an initial AP adaptation (Fig. 2A, bottom green trace; Fig. 2D, green dots), and the rising AP slope showed a single acceleration phase (Figs. 2C, 3B). In 77% of IN_{CCK} we observed a decrease in AP amplitude starting from the second AP of the discharge (Fig. 2A, arrow, first row; Karson et al., 2009; Goff and Goldberg, 2019). As for IN_{PV} , IN_{CCK} showed a lower MRS compared with $IN_{SOM4/5}$ and PYR cells (Fig. 3E). Sc-dPCR performed in 12 of 13 IN_{CCK} -confirmed CCK cDNA in these cells (green dots Fig. 4B, green dots). In eight of IN_{CCK} , cDNA for *PV* and *SOM* was also found (Fig. 4B, red and blue dots). Firing properties were not different in IN_{CCK} recorded from superficial and deep EC layers.

IN_{SOM} features have been described in the EC (Neske et al., 2015; Ferrante et al., 2017; Kecskés et al., 2020; Fernandez et al., 2022). In line with Neske et al. (2015), two different types of presumed somatostatinergic cells (IN_{SOM}) were recorded in

superficial and deep EC layers, (1) superficial layer $IN_{SOM2/3}$ ($n = 6$; Fig. 2A–C, middle column, light blue) featured slowly adapting APs (Fig. 2D,E, light blue dots) without AHP and (2) a single-phase AP acceleration (Figs. 2C, 3B); deep layer $IN_{SOM4/5}$ ($n = 9$; Fig. 2A–C, blue) showed fast-rising nonadapting APs that sustained a very high firing rate (>100 Hz) during injection of large amplitude depolarizing current steps. APs in $IN_{SOM4/5}$ were followed by fast AHPs (Fig. 2A, asterisk, blue trace). Unlike $IN_{SOM2/3}$, deep layer $IN_{SOM4/5}$ featured a double AP slope acceleration (Figs. 2C, 3B, arrowheads). Finally, $IN_{SOM4/5}$ showed a significantly greater MRS than IN_{PV} , IN_{CCK} , and PYRs (Fig. 3E) and a significantly faster repolarization compared with all IN subtypes and PYRs (Fig. 3F). Sc-dPCR revealed SOM cDNA in IN_{SOM} of both superficial and deep layers ($n = 12$ IN_{SOM}), with minor content of both PV and CCK cDNA (Fig. 4C, red and green dots). PYR neurons ($n = 10$; Fig. 2A–C, black lines and drawings) generated adapting APs (Fig. 2A,D,E) with no AHPs and showed maximal firing rate below 20 Hz. Average maximal AP amplitude in PYRs was significantly higher in comparison with all INs (Figs. 2C, 3D).

As sc-dPCR showed higher cDNA copies of CCK than PV in 4 of 11 IN_{PV} , we further analyzed electrophysiological features in these 4 IN_{PV} (Fig. 4). Their I/O curves, AP adaptation features, and AP phase plots (Fig. 4D,E, purple dots; Fig. 4F, purple line) were identical to the other IN_{PV} cells (red dots and line) but were different from IN_{CCK} (green dots and line). As shown in Figure 1D, most INs recorded from GAD67 mice were either IN_{SOM} (100%) or IN_{PV} (85.7%), whereas fluorescent INs in slices from GAD65 mice were mainly (83.33%) IN_{CCK} . The percentage of IN_{PV} , IN_{CCK} , and IN_{SOM} recoded in superficial layers (2 and 3) or deep layers (4 and 5) of the EC are illustrated in Fig. 1E.

Activity of interneurons and pyramidal cells during 4-AP-induced SLEs

Simultaneous extracellular and intracellular INs recordings were performed in control conditions and during perfusion with medium containing 100 μ M 4-AP, which in all slices induced SLEs. Interestingly, during 4-AP application, all recorded INs were very active before and during all phases of SLEs. In all INs, subthreshold spontaneous activity was observed during 4-AP perfusion (Fig. 5A,C, arrowheads) in parallel with increased background activity observed in the LFP recording (Fig. 5D). As commonly observed in brain slices in control conditions, INs show no or very sporadic AP firing before 4-AP (Fig. 5F, top, control condition); however, within 10 min after 4-AP perfusion onset, AP firing was observed in 78.2% of INs during the pre-SLE period (Fig. 5E, bottom). In the 180 s before SLE onset, preictal AP firing was seen in 13 of 17 IN_{PV} (Fig. 5F, red dots), in 9 of 13 IN_{CCK} (green dots), and in 10 of 15 IN_{SOM} (blue dots). Interictal APs superimposed on a large amplitude synaptic event were observed in 7.5% of IN_{PV} , 92.3% of IN_{CCK} (Fig. 5A,D, example) and in 80% of IN_{SOM} , respectively. Virtually all INs were entrained during SLEs (96%). Unlike INs, PYRs showed neither enhanced synaptic activity nor spontaneous firing during 4-AP before SLEs (Fig. 5D,F, black dots).

Field potential preictal spikes were observed ahead of SLEs in all experiments; INs generated either single APs or AP burst that was superimposed on a depolarizing potential and correlated with field preictal spikes (Fig. 5A,C,D). The 4-AP-induced preictal epileptiform discharges, identified with field potential recordings in a subset of experiments ($n = 7$), were not modified by coprefusion with either 3 mM kynurenic acid (a broad spectrum glutamatergic antagonist, $n = 4$) or 10 μ M DNQX (a selective non-

NMDA glutamatergic antagonist) plus 10 μ M D-CPP (a competitive NMDA antagonist, $n = 3$), and were abolished by 4-AP coprefusion with 100 μ M GABA_A receptor blocker picrotoxin (PTX; $n = 7$; Fig. 6A). In addition, interictal spikes were generated during coprefusion of 100 μ M 4-AP and 100 μ M PTX (Fig. 6B, arrowheads), but SLEs were not observed ($n = 9$). Reperfusion of 4-AP after PTX washout (Fig. 6B, right) promoted an increase of background synaptic noise (which was occluded by the simultaneous PTX plus 4-AP perfusion) that culminated with an SLE ($n = 7$).

In line with previous reports (Boido et al., 2014a; Avoli et al., 2016), 4-AP-induced SLEs were characterized by a continuum of patterns that included both LVF and HYP onsets (see below, Discussion). Specifically, we identified as LVF the SLEs that did not present with large spikes before the low-voltage activity (Fig. 5A,B, representative examples, $n = 29$) and as HYP the SLEs with large amplitude extracellular spikes at onset (Fig. 5C,D; $n = 15$). Extracellular recordings confirmed that both LVF and HYP SLEs were superimposed on a large amplitude, negative slow potential deflection likely because of changes in extracellular potassium concentration (Avoli et al., 1996a,b; Gnatkovsky et al., 2008; Librizzi et al., 2017). All recorded INs were active from the very onset of both SLE types. LVF onset SLE patterns were recorded in 70.6% IN_{PV} , 54% IN_{CCK} , 50% IN_{SOM} , and 80% PYRs; HYP SLE onset patterns were recorded in 29.4% IN_{PV} , 46% IN_{CCK} , 50% IN_{SOM} , and 20% PYRs.

Next, we analyzed the temporal correlation between LFP onset of SLE and the activity of PYR and IN subtypes. As illustrated in Figure 7, A and B, we used two measures to evaluate the delay between neuronal activity and the extracellular discharge. First, we calculated the delay between the first AP of the ictal discharge and the onset of the slow deflection associated with either LVF (Fig. 7A) or the HYP onset SLEs (Fig. 7B; Fig. 7Aa,Ba, the expanded trace, Ca, plot). The second parameter was the delay between the first intracellular depolarizing potential recorded at SLE onset and the initiation of the slow field potential deflections occurring at LVF or HYP onset SLEs (Fig. 7Ab,Bb,Cb,D, plots). Both delays *a* and *b* were negative or close to zero for all IN subtypes and were positive in most PYRs. As illustrated in Figure 7D for parameter *b*, $IN_{SOM4/5}$, $IN_{SOM2/3}$, and IN_{CCK} fired action potentials before the extracellular SLE (time 0), whereas IN_{PV} became active just before or after the extracellular SLE onset. Statistical analysis showed that IN_{SOM} activity consistently started before PYRs (Fig. 7Cb, right, asterisks). These data demonstrate that during both LVF and HYP SLEs induced by 4-AP in the mouse EC, IN_{SOM} are active earlier than PYRs. These findings also suggest that PYRs activity is entrained into seizure generation after IN_{CCK} , IN_{SOM} , and IN_{PV} activities.

During SLEs, depolarizing blockade (DB; Fig. 8A, arrowhead) of AP firing was observed in 37.5% IN_{PV} , in 50% IN_{CCK} , 44.4% IN_{SOM} , and in 40% PYRs (Fig. 8B). DB was observed at the beginning of both LVF and HYP SLEs and lasted 4.56 ± 1.36 s, 3.97 ± 2.20 s, and 3.64 ± 1.06 s in IN_{PV} , IN_{CCK} , and IN_{SOM} , respectively (Fig. 8D). Compared with INs, DB duration in PYRs was shorter (0.95 ± 0.19 s; Fig. 8D). DB was consistently observed only in INs and PYRs in which membrane potential depolarized above -30 mV during SLE onset (Fig. 8C). As SLEs progressed, firing resumed after DB in all IN subtypes. During the last phases of the SLEs, sustained AP firing was consistently observed in all INs and PYRs. Except for a subgroup of INs (see below), intracellular bursting activity was synchronized with the LFP bursting observed during the late stage of SLEs (Aracri et al., 2006; Boido et al., 2014b).

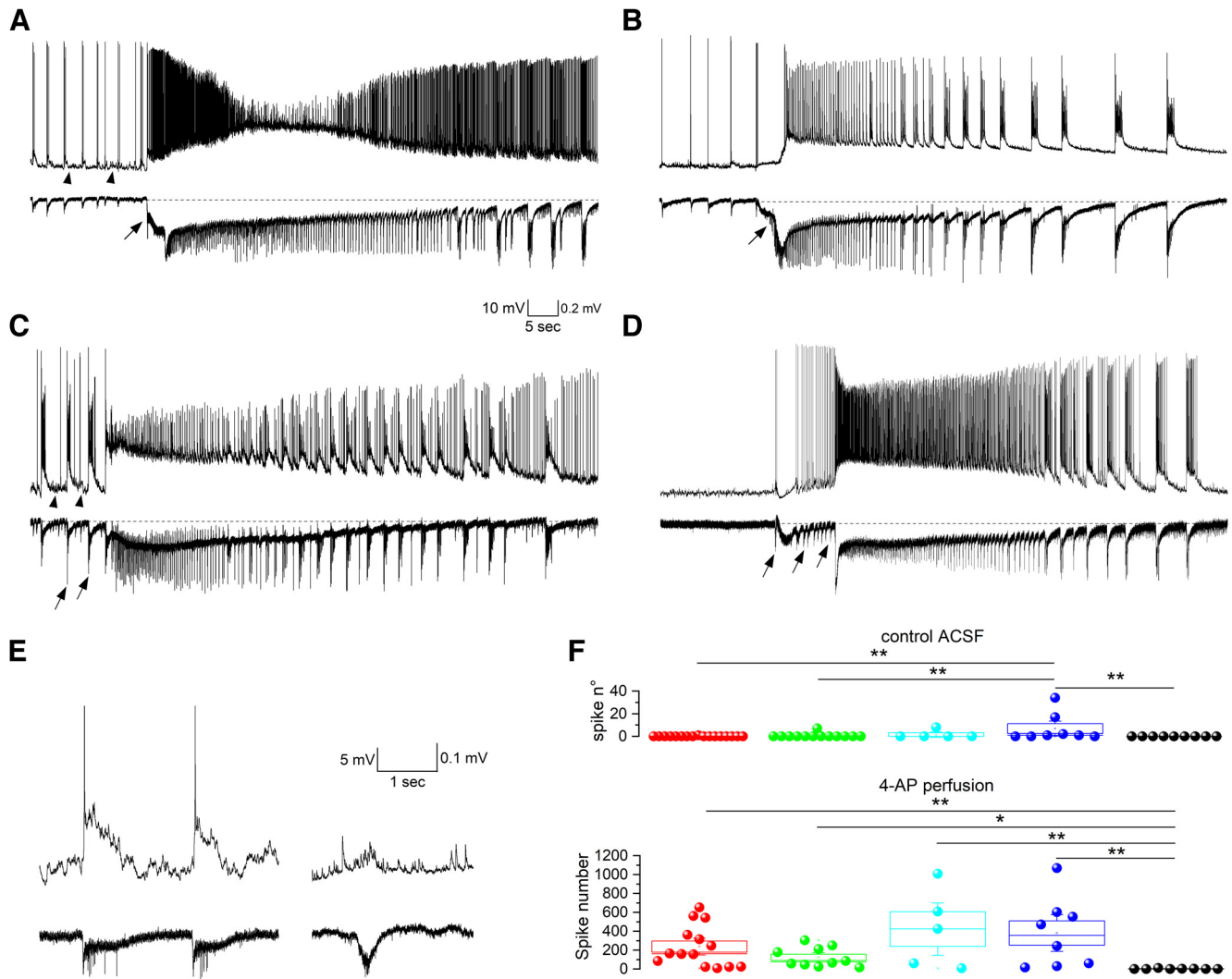


Figure 5. Firing patterns of interneurons and pyramidal cells during SLEs induced by slice perfusion with $100 \mu\text{M}$ 4-AP in 0.5 mM Mg^{2+} . **A**, LVF (arrow) SLE simultaneously recorded with an extracellular electrode (bottom trace) and from an IN_{PV} (top trace). **B**, LVF-onset SLE (arrow) simultaneously recorded from a PYR neurons (top trace) and with an extracellular electrode (bottom trace). **C**, SLE characterized by an HYP (arrows on large spikes in bottom trace) intracellularly recorded from an IN_{SOM} (top trace). Arrowheads point to synaptic background activity generated during 4-AP perfusion (**E**). **D**, HYP SLE recorded from an PYR (top trace). **E**, Simultaneous extracellular (bottom traces) and intracellular (top traces) recordings during the preictal activity observed in an IN_{PV} (**A**) and an IN_{CCK} (**B**); spontaneous synaptic activity was observed in correlation with extracellular preictal spikes. **F**, Top, Quantification of AP numbers during 3 min perfusion with control ACSF before 4-AP application in IN_{PV} (237 ± 58.66 , $n = 15$, red dots), IN_{CCK} (124.20 ± 32.49 , $n = 11$, green dots), $\text{IN}_{\text{SOM2/3}}$ (1.6 ± 1.6 , $n = 5$, cyan dots), $\text{IN}_{\text{SOM4/5}}$ (6.87 ± 4.37 , $n = 8$, blue dots) and in PYRs (2.5 ± 1.43 , $n = 9$, black dots). Bottom, Quantification of AP numbers during in 4-AP, 3 min before the onset of SLEs; IN_{PV} (237 ± 58.66 , $n = 15$, red dots), IN_{CCK} (124.20 ± 32.49 , $n = 11$, green dots), $\text{IN}_{\text{SOM2/3}}$ (421.4 ± 184.3 , $n = 5$, cyan dots), $\text{IN}_{\text{SOM4/5}}$ (380.37 ± 129.38 , $n = 8$, blue dots), and in PYRs (2.5 ± 1.43 , $n = 9$, black dots). Kruskal–Wallis test with Dunn's *post hoc* test (* = $p < 0.05$, ** = $p < 0.01$, *** = $p < 0.001$).

We identified three different seizure end patterns that are illustrated in Figure 9A and quantified in the graph in Figure 9B. Short AP bursts synchronous to the LFP burst (Fig. 9Aa,9B, black columns) were prominent in PYRs (66.66%), were present in 25% IN_{SOM} , and were sporadically observed in IN_{PV} (9%) and IN_{CCK} (7.6%). Virtually all IN_{CCK} generated a robust bursting discharge that extended beyond the duration of the simultaneously recorded extracellular burst discharge (Fig. 9Ab,C, striped columns). This type of pattern was observed also in 54.5% IN_{PV} , 41.66% IN_{SOM} , and 33.34% PYRs. Finally, high-frequency firing was observed exclusively in IN_{PV} (36.5%) and IN_{SOM} (36.34%; Fig. 9Ac,C, empty columns); a burst discharge synchronous with the LFP burst was nested within the high-frequency barrage (Fig. 9Bc). Interestingly, DB was observed also in one of six IN_{PV} and two of four IN_{SOM} that displayed a continuous high-frequency firing. Late bursting patterns were observed in both LVF and HYP SLEs.

Discussion

The present study provides new evidence for the role of different IN subpopulations in the generation of seizure-like discharges induced by acute 4-AP treatment in the *in vitro* mouse EC slice preparation. Our findings demonstrate that 4-AP-induced SLEs (1) are preceded by enhanced INs firing leading to GABAergic preictal spikes; (2) are abolished by co-perfusion of 4-AP with the GABA receptor antagonist picrotoxin; (3) initiate with the activation of IN_{PV} , IN_{CCK} , and IN_{SOM} , followed by the recruitment of PYRs; and (4) are also characterized by intense involvement of all IN subtypes throughout their development and termination.

Early studies have reported that the onset of SLEs induced by 4-AP in EC slices is associated with a synchronous field potential that likely mirrors INs activity (Avoli et al., 1993, 1996a; Lopantsev and Avoli, 1998b). These results were later confirmed and were reproduced in several experiments, including hippocampal and EC

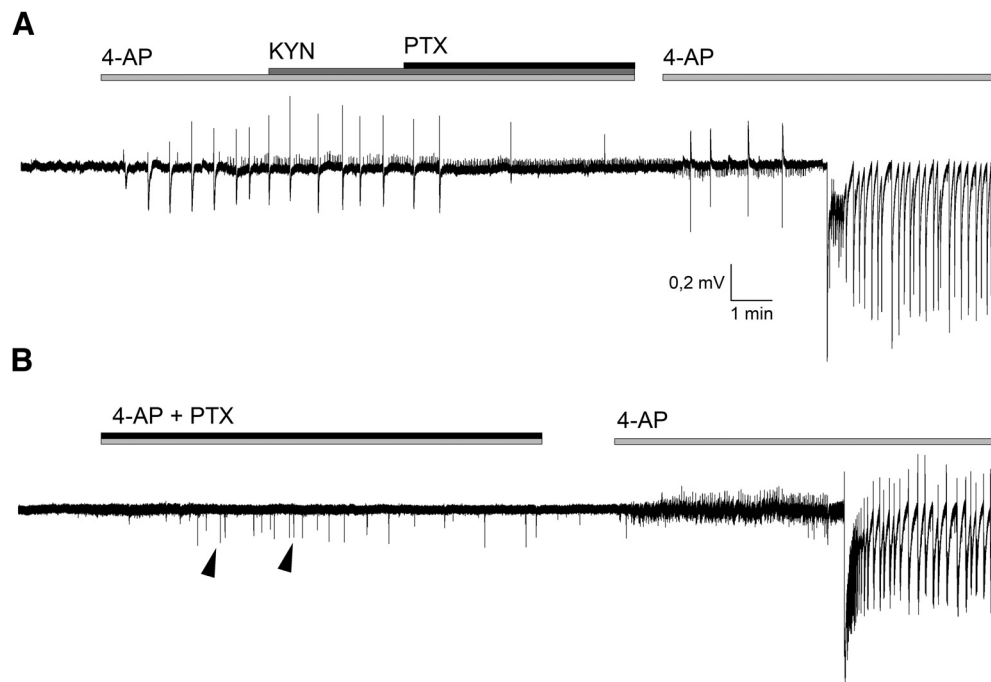


Figure 6. GABA_A receptor dependence of epileptiform events induced by 4-AP. **A**, Field potential extracellular recordings during 4-AP (light gray bar), perfused with kynurenic acid (KYN; dark gray bar) and coperfused with kynurenic acid and picrotoxin (PTX; black bar). **B**, Field extracellular recordings during 4-AP (light gray bar) perfused with PTX (black bar) and with 4-AP alone (right).

slices from different rodents and the isolated guinea pig brain preparation (for review, Avoli and de Curtis, 2011; Kaila et al., 2014; de Curtis and Avoli, 2016; Devinsky et al., 2018). SLE initiation by INs was confirmed in neocortex, hippocampus, and EC *in vitro* after exposure to 4-AP (Gnatkovsky et al., 2008; Uva et al., 2009, 2015, 2017a; Avoli et al., 2016; Librizzi et al., 2017; Lado et al., 2022), low bicuculline concentration (Gnatkovsky et al., 2008; Uva et al., 2015), low-Mg²⁺/high-K⁺ solution (Dzhala and Staley, 2003; Ziburkus et al., 2006; Laszóczi et al., 2009), as well as following high-frequency stimulation (Kaila et al., 1997; Velazquez and Carlen, 1999; Fujiwara-Tsukamoto et al., 2007). Overall, these studies indicate that GABAergic network hyperactivity is common at the onset of *in vitro* SLEs generated acutely following diverse experimental manipulations, and it is thus not observed only during 4-AP treatment.

INs activity at seizure onset was confirmed by single-unit and multiunit *in vivo* recordings performed in models of temporal lobe epilepsy (Grasse et al., 2013; Fujita et al., 2014; Toyoda et al., 2015) and in patients with focal epilepsies (Truccolo et al., 2011; Elahian et al., 2018; Weiss et al., 2019; Merricks et al., 2021). Interestingly, hyperactivity of GABAergic neurons is also involved in the initiation of other pathologic network activities, such as migraine-related cortical spreading depolarization (Chever et al., 2021; Lemaire et al., 2021).

The 4-AP focal seizure model

The 4-AP *in vitro* model has been used to study cellular seizure mechanisms in temporal lobe structures. We noticed that in the *in vitro* 4-AP model, a continuum of patterns that included LVF- and HYP-onset SLEs was recorded, and in particular HYP onset patterns were often followed by a LVF phase. Regardless of the onset pattern, INs firing started at SLE onset or just before it, and for these reasons we did not proceed with a separate analysis in LVF and HYP SLEs. Similar electrographic SLE features were obtained also by systemic 4-AP treatment *in vivo* (Lévesque et

al., 2013) and by perfusing 4-AP in the *in vitro* isolated guinea pig brain preparation. Interestingly, HYP seizures were recorded more frequently in TLE models *in vivo* (Lévesque et al., 2012) and in the human TLE associated with hippocampal sclerosis (Ogren et al., 2009; Weiss et al., 2019). *In vivo* studies suggest that HYP SLEs are initiated by principal cells and are sustained by glutamatergic transmission (Salami et al., 2015). Unlike *in vivo* conditions, previous reports by our groups (Köhling et al., 2016; Librizzi et al., 2017) showed that not only LVF SLEs but also HYP SLEs in 4-AP-treated EC slices are initiated by enhanced INs activity; these findings are confirmed in the present report.

Our study analyzed 4-AP-induced network activities on naive EC-hippocampal slices obtained from nonepileptic animals. The use of *in vitro* slices from chronically epileptic animals could be considered a better option to analyze the microcircuitry involved in SLEs generation. However, *in vitro* brain slices do not generate seizures spontaneously; this aspect makes the use of brain tissue slices from chronic TLE animals impractical to analyze cellular network interactions during SLEs because proepileptic drugs would be, in any case, necessary to induce epileptiform discharges. This is an intrinsic limitation of *in vitro* experimental studies of ictogenesis that cannot be bypassed.

GABAergic interneuron phenotyping

We used EC slices obtained from GAD65 or GAD67 mice, which express GFP exclusively in GABAergic interneurons (Tamamaki et al., 2003; López-Bendito et al., 2004). Several studies demonstrated that cortical INs can be identified by electrophysiological features (Freund and Buzsáki, 1996; Kawaguchi and Kondo, 2002; Rudy et al., 2011; Urban-Ciecko and Barth, 2016; Pelkey et al., 2017). IN_{PV}, IN_{CCK}, and IN_{SOM} firing features described in rodent EC (Varga et al., 2010; Neske et al., 2015; Armstrong et al., 2016; Ferrante et al., 2017; Fernandez et al., 2022) are similar to those reported for other cortical areas and for the hippocampal region (Pelkey et al., 2017). Parameters usually considered

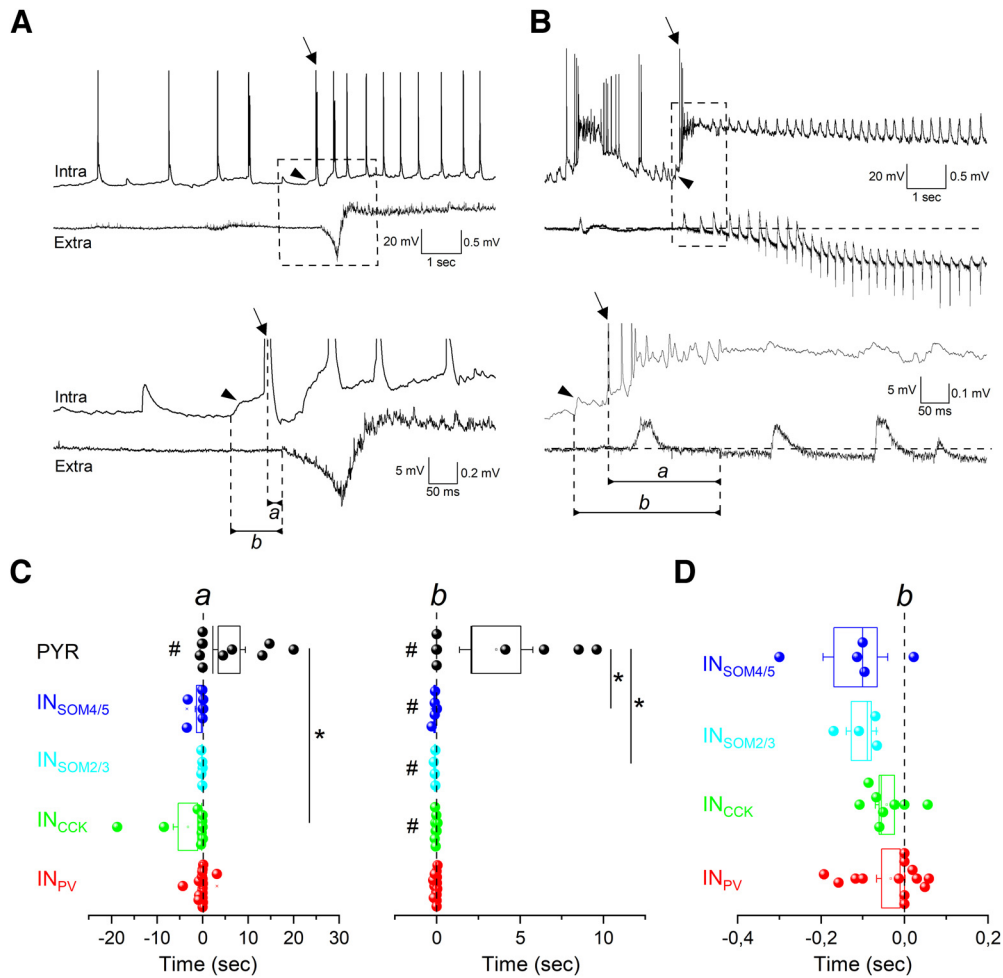


Figure 7. Correlation between extracellular SLE onset and the activity of INs and PYRs. **A–Cb**, Low-voltage fast SLE simultaneously recorded with an extracellular electrode (bottom trace) and an $IN_{SOM2/3}$ (top trace). Bottom, Expanded version of the dashed square. Arrows indicate the first action potential peak; the arrowhead points to the onset of depolarization; the right dashed line marks SLE onset (slow deflection onset) in the extracellular trace. Measurements **a** and **b** are illustrated in **Ca** and **Cb**, respectively. **Ba,b**, The measurements in a HYP SLE recorded from a IN_{CCK} . **Ca**, Delays between the peak of the first ictal AP (arrows) and the onset of the extracellular slow deflection at SLE onset (time 0, dotted vertical line); IN_{PV} (-204.92 ± 332.16 ms, $n = 16$, red dots), IN_{CCK} (-3135.93 ± 2099.16 ms, $n = 9$, green dots), $IN_{SOM2/3}$ (-125.6 ± 61.8 ms, $n = 5$, cyan dots), and $IN_{SOM4/5}$ (-800.13 ± 556.79 ms, $n = 8$, blue dots); PYRs showed a higher variability ($+5824.1 \pm 2388.25$ ms, $n = 10$, black dots). AP firing showed statistical significance for IN_{CCK} in comparison with PYR (right, asterisk; Kruskal–Wallis test with Dunn’s *post hoc* test). Wilcoxon signed-rank test showed that PYR began to fire after onset of SLE (positive delay; hashtag symbol on the left of the box chart), whereas INs did not have significant delay (started to fire at onset of SLE). **Cb**, Plot of the delays between the preictal intracellular depolarizing potential (arrowheads) and the onset of the slow extracellular deflection at SLE onset (time 0); IN_{PV} (-32.82 ± 22.55 ms, $n = 13$), IN_{CCK} (-42.71 ± 18.37 ms, $n = 8$), and $IN_{SOM2/3}$ (-103.75 ± 24.12 ms, $n = 4$) and $IN_{SOM4/5}$ (-117.6 ± 51.74 ms, $n = 5$); PYRs ($+3579.08 \pm 1464.22$ ms; $n = 8$). $IN_{SOM2/3}$ and $IN_{SOM4/5}$ began to fire earlier than PYRs (asterisks on the right of box charts; Kruskal–Wallis test with Dunn’s *post hoc* test). Wilcoxon signed-rank test showed that PYR began to fire after onset of SLE (positive delay), whereas IN_{CCK} , $IN_{SOM2/3}$ and $IN_{SOM4/5}$ began to fire before onset of SLE (negative delay), and IN_{PV} did not have significant delay (started to fire at onset of SLE). **D**, Same data as in **Cb**, illustrated with an extended time scale and without PYRs data for better comparing features of GABAergic neurons; symbols for statistical significance are not indicated; * = $p < 0.05$.

reliable for INs phenotyping include AP features, firing discharge, and adapting properties. We classified the recorded INs according to these criteria. Another INs marker is the cDNA content revealed by sc-dPCR. We demonstrated here that INs contain different amounts of PV and CCK cDNA. This coexpression most likely reflects the high sensibility of digital PCR technique.

Studies that used single-cell reverse transcription PCR techniques have shown that ~40% of fast-spiking INs and 55% of pyramidal cells recorded in cortical slices express CCK cDNA (Gallopín et al., 2006). Whether the transcript expression of two different peptides in INs reflects CCK-GABA neuron identity has been questioned (Tricoire et al., 2011). Furthermore, this article highlights how several types of hippocampus INs coexpress PV and CCK transcripts. Another evidence of this coexpression is reported in human epileptic tissue, where 28% of CCK INs also express PV peptide (Zhu et al., 2018). As reported in Figure 4,

INs with high PV and CCK coexpression were classified as IN_{PV} based on membrane and firing properties. Our analysis demonstrates that the electrophysiological characterization is the most reliable identifier to stratify IN subtypes. Of note, INs clustering according to electrophysiological criteria showed that the variability of both input/output curve and average phase plots values were minimal, as shown in Fig. 2, B and C, suggesting a high homogeneity of firing patterns within each identified IN subgroups.

Interneuron activity during preictal and SLE dynamics

IN subtypes have been studied in the EC and in the hippocampus (Tremblay et al., 2016; Pelkey et al., 2017). IN_{PV} form perisomatic contacts with principal cells broadly distributed throughout EC layers (Beed et al., 2013; Couey et al., 2013; Fuchs et al., 2016; Kecskés et al., 2020) by targeting the soma and the action

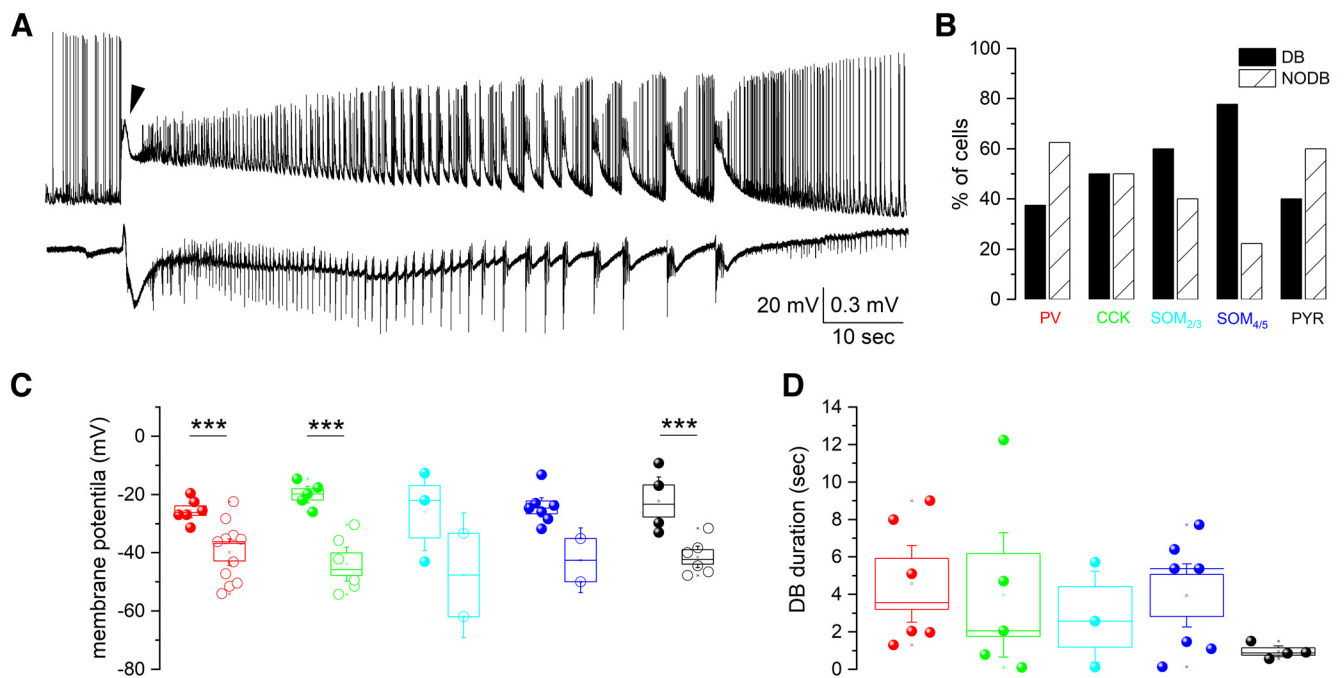


Figure 8. Depolarizing block after SLEs induced by 4-AP. **A**, Representative LVF SLE recorded with an extracellular electrode (bottom trace) and with a patch electrode from an IN (top trace); the arrowhead indicates the DB after SLE onset. **B**, Percentage of cells that showed DB (IN_{PV} = 37.5%, IN_{CCK} = 50%, IN_{SOM_{2/3}} = 60%, IN_{SOM_{4/5}} = 80% and PYRs = 40%, black columns) and did not show DB (IN_{PV} = 62.5%, IN_{CCK} = 50%, IN_{SOM_{2/3}} = 40%, IN_{SOM_{4/5}} = 20% and PYRs = 60%, striped columns). **C**, Quantification of maximal membrane potential depolarization value measured in IN_{PV}, IN_{CCK}, and IN_{SOM} during SLE; membrane potential values of INs that show (left columns) and did not show DB (right columns) are illustrated (* = $p < 0.05$, *** = $p < 0.001$). All INs with DB showed membrane depolarization above -30 mV. Statistical analysis could not be performed for IN_{SOM_{2/3}} and IN_{SOM_{4/5}} because of the small sample size. **D**, DB duration in seconds (sec) in IN_{PV} (4.56 ± 1.36 , $n = 6$, red dots), IN_{CCK} (3.97 ± 2.20 , $n = 5$, green dots), IN_{SOM_{2/3}} (2.8 ± 1.62 , $n = 3$, cyan dots), IN_{SOM_{4/5}} (3.93 ± 1.12 , $n = 7$, blue dots), and PYRs (0.95 ± 0.19 , $n = 4$, black dots). The data show no significant difference in the duration of the DB. ANOVA with Tukey's *post hoc* test was used.

potential initiation zone; therefore, these cells are in a unique position to control the occurrence and the timing of postsynaptic cell AP firing. IN_{SOM} and some IN_{CCK} preferentially target dendrites of principal neurons with higher density in layers III–V (Fuchs et al., 2016; Tremblay et al., 2016; Kecskés et al., 2020), where they are proposed to gate and modulate excitatory inputs (Urban-Ciecko and Barth, 2016). Although IN_{CCK} have not been specifically studied in the EC, it is well known that they form synaptic contacts both on the soma and on the apical dendrites of postsynaptic principal cells in neocortex (Nguyen et al., 2020). Interestingly, EC IN_{PV} are interconnected through reciprocal synaptic interactions and gap junctions (Hjorth et al., 2009; Fernandez et al., 2022). IN_{PV} and IN_{SOM} are also synaptically connected in the hippocampus (Karson et al., 2009). Moreover, IN_{SOM} are coupled via gap junctions with other INs, but not with other IN_{SOM} (Pfeffer et al., 2013; Fernandez et al., 2022). This intra-INs connectivity forms functional interactions that are crucial to sustain GABAergic neuronal network activity, including neuronal oscillations (Klausberger et al., 2005; Cardin et al., 2009) and likely focal seizures.

We demonstrated here that background firing during 4-AP application is enhanced in INs, but not in PYRs. Accordingly, preictal spiking activity induced by 4-AP was blocked by GABAergic antagonists but not by glutamatergic receptor antagonists (Uva et al., 2013). As we observed enhanced synaptic activity exclusively in INs, we assumed that increased spontaneous synaptic events are mediated by the prolongation of AP depolarization (Mitterdorfer and Bean, 2002) induced by the potassium channel blocker 4-AP that may facilitate IN-to-IN synaptic interactions.

At seizure onset, INs AP firing was enhanced. Although all INs fire in coincidence with SLE onset, IN_{SOM} were activated

first ahead of the SLE initiation as identified in field potential recordings. It should be mentioned that the exact identification of the extracellular seizure onset is not trivial. Still, the two methods we used to correlate both intracellular activities with the extracellular population discharge resulted in a clear divergent trend between INs and PYRs and suggest that PYRs activate after INs and after the extracellular SLE initiation. Similar conclusions were reached during studies performed in EC mouse slices (Cammarota et al., 2013; Librizzi et al., 2017), which demonstrated a consistent precession of INs activity during 4-AP-induced SLEs with simultaneous double recordings from pairs of INs and PYRs.

LVF seizure onset could be induced by optogenetic activation of IN_{PV} or IN_{SOM} in the 4-AP hippocampal and neocortical slice model (Shiri et al., 2015; Yekhele et al., 2015; Chang et al., 2018) and in naive and pilocarpine-treated mice that express channelrhodopsin in IN_{PV} or IN_{SOM} (Shiri et al., 2015, 2016; Assaf and Schiller, 2016; Miri et al., 2018). On the other hand, optogenetic inhibition of PYRs has been shown to reduce or prevent seizures in many seizure models (Chiang et al., 2014). A recent study reported that different IN subtypes control SLEs in somatosensory mouse cortex slices (Lado et al., 2022); in the presence of 4-AP, light activation of channelrhodopsin-expressing IN_{PV} and IN_{SOM} (but not IN_{VIP}) evoked epileptiform discharges, suggesting that INs contribute differently to the initiation and inhibition of epileptiform discharges in cortical networks. However, to identify the relevance of specific IN subtypes in SLE initiation chemogenetic or optogenetic silencing will be required in future experiments.

We confirmed the presence of DB in a subgroup of INs during both LVF and HYP SLEs (Cammarota et al., 2013). It is interesting to note that DB showed a clear trend to be much longer

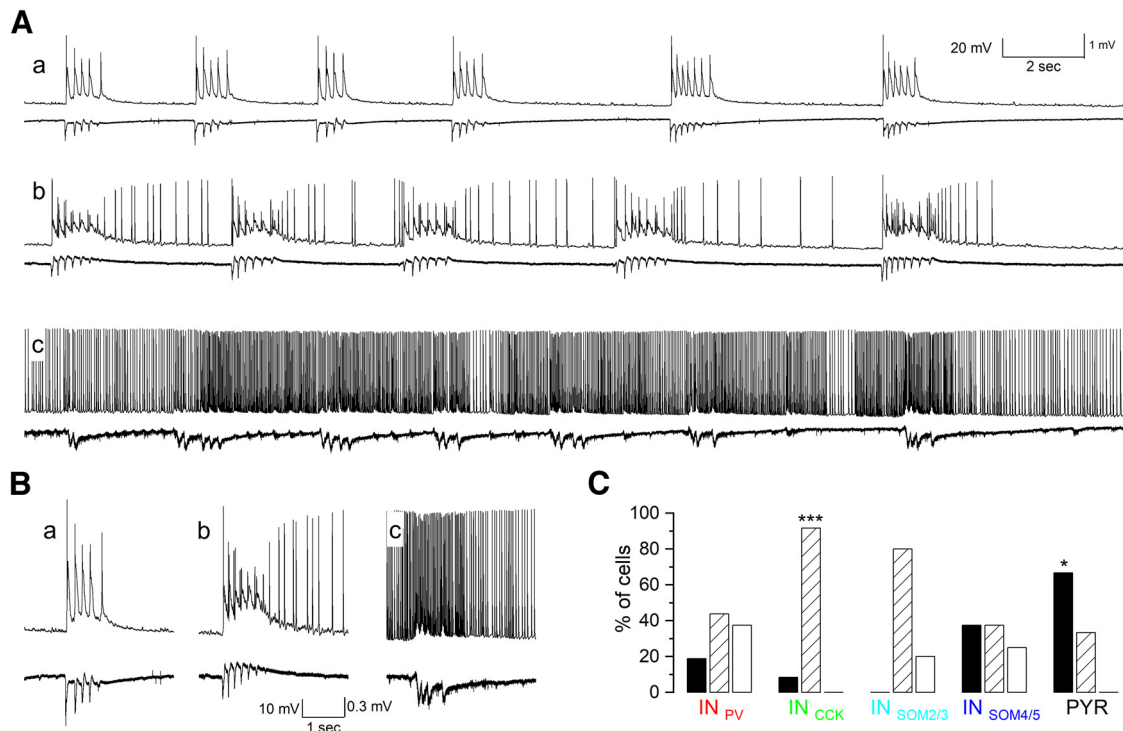


Figure 9. Different firing patterns during the late phase at the end of SLEs. *Aa–c*, Burst firing recorded with the whole-cell patch electrodes (top traces) or the extracellular electrodes (bottom traces) during the late phase of SLEs induced by 4-AP perfusion. In the IN illustrated in *a*, the duration of the extracellular and intracellular bursts are similar. Intracellular burst firing lasted longer than the simultaneous extracellular burst discharge in the IN shown in *b*. High-frequency firing not related with extracellular bursting activity of SLEs was recorded from the IN in *c*. *B*, Expanded traces of the three different late SLE patterns illustrated in *A*. *C*, Percentage of neurons (IN_{PV}, IN_{CCK}, IN_{SOM2/3}, IN_{SOM4/5}, and PYRs) showing the three patterns displayed in *A*. Short bursts were recorded in 18.75% IN_{PV}, 8.33% IN_{CCK}, 0% IN_{SOM2/3}, 37.5% IN_{SOM4/5}, and 66.66% PYRs (black columns); long-lasting intracellular bursts were observed in 43.75% IN_{PV}, 91.66% IN_{CCK}, 80% IN_{SOM2/3}, 37.5% IN_{SOM4/5}, and 33.33% PYRs (striped columns); high-frequency firing not correlated with extracellular bursting was found in 37.5% IN_{PV}, 0% IN_{CCK}, 20% IN_{SOM2/3}, 25% IN_{SOM4/5} and 0% PYRs (empty columns). Chi-square goodness-of-fit test showed that PYRs displayed more short burst discharges than other types of firing ($p = 0.049$) and IN_{CCK} more long-lasting intracellular bursts than other types of firing ($p = 0.0001$); IN_{PV} and IN_{SOM} did not show a favorite type of firing.

(3–4 s) in INs in comparison with PYRs (<1 s). The possibility that the reduction in INs firing during DB could be responsible for the transition from a preictal condition of INs hyperactivity into the SLEs has been proposed in the past in the high-K⁺ and 4-AP models (Ziburkus et al., 2006; Cammarota et al., 2013). The permissive action of interneuronal DB to start seizures is not supported by our observation that only ~50% of INs undergo DB, and also PYRs display DB. In addition, SLE as extracellular population phenomenon initiates before DB develops. Based on previous experimental findings, we propose that DB is a cellular phenomenon associated with the abrupt neuronal depolarization beyond AP regeneration, possibly mediated by the fast changes in extracellular potassium generated by INs activity at seizure onset (Gnatkovsky et al., 2008; Trombin et al., 2011). Not surprisingly, we demonstrated that the presence of DB in individual INs depends on membrane potential depolarization level reached during SLE onset: when membrane potential returns to values suitable with reactivation of AP firing, SLEs progress into a phase of irregular AP firing that is followed within seconds by the buildup of bursting activity that characterizes the final phase of a seizure (Devinsky et al., 2018).

Finally, we confirmed an important finding that has been reported by several *in vitro* studies but seldom highlighted and discussed; all recorded INs generated robust firing throughout the late SLE phases. About one-third of IN_{PV} and IN_{SOM} continuously fire high-frequency APs from the onset of SLEs to its end, without evidence of DB. The large majority of INs discharged robust burst firing in synchrony with the local field potential bursting discharges observed with extracellular electrodes. Bursts

during late SLEs are longer than field bursts in >90% IN_{CCK}, >50% IN_{PV}, and in >40% IN_{SOM}, and was observed in ~30% PYRs; the excessive firing during long IN bursts, together with high-frequency firing observed in one-third of IN_{PV} and IN_{SOM} could be responsible for the interburst depression observed in this late SLE phase and could contribute to SLE termination.

An alternative mechanism that links neuronal hyperactivity to seizure termination was recently proposed; the massive bursting of IN networks together and in synchrony with PYRs may produce a brief and transient condition of neuronal hyperactivity, followed by a synchronous postburst depression mediated by both synaptic and extrasynaptic events. When highly synchronous postburst depression ensues, the synchrony of the next burst is enhanced, and the duration of the next postburst depression progressively increases. As synchrony increases, the interburst interval gets progressively longer up to a critical point when the reactivation of a further burst is hampered; this mechanism may lead seizures to stop (Boido et al., 2014a; Uva et al., 2021).

Conclusions

In the *in vitro* 4-AP model of temporal lobe seizures, PV, CCK, and SOM INs are very active at SLE onset, with IN_{SOM} consistently heralding the local field potential SLE initiation. INs are very active throughout all SLE phases, and only ~50% show DB. This finding suggests that GABAergic INs rundown is not required to boost seizure initiation and progression. Finally, INs hyperactivity in synchrony with PYRs may contribute to seizure termination. The acute 4-AP model generates SLEs that mimic

seizure patterns commonly observed in human focal epilepsy and reproduces neuronal activities observed in patients during presurgical intracerebral monitoring. Based on this evidence, the 4-AP model represents an excellent model to generate working hypotheses for future validation studies to be performed in different *in vivo* models and in humans.

References

- Aracri P, Colombo E, Mantegazza M, Scalmani P, Curia G, Avanzini G, Franceschetti S (2006) Layer-specific properties of the persistent sodium current in sensorimotor cortex. *J Neurophysiol* 95:3460–3468.
- Armstrong C, Wang J, Yeun Lee S, Broderick J, Bezaire MJ, Lee SH, Soltesz I (2016) Target-selectivity of parvalbumin-positive interneurons in layer II of medial entorhinal cortex in normal and epileptic animals. *Hippocampus* 26:779–793.
- Assaf F, Schiller Y (2016) The antiepileptic and ictogenic effects of optogenetic neurostimulation of PV-expressing interneurons. *J Neurophysiol* 116:1694–1704.
- Avoli M, de Curtis M (2011) GABAergic synchronization in the limbic system and its role in the generation of epileptiform activity. *Prog Neurobiol* 95:104–132.
- Avoli M, Psarropoulou C, Tancredi V, Fueta Y (1993) On the synchronous activity induced by 4-aminopyridine in the CA3 subfield of juvenile rat hippocampus. *J Neurophysiol* 70:1018–1029.
- Avoli M, Barbarosle M, Lücke A, Nagao T, Lopantsev V, Köhling R (1996a) Synchronous GABA-mediated potentials and epileptiform discharges in the rat limbic system *in vitro*. *J Neurosci* 16:3912–3924.
- Avoli M, Louvel J, Kurcewicz I, Pumain R, Barbarosie M (1996b) Extracellular free potassium and calcium during synchronous activity induced by 4-aminopyridine in the juvenile rat hippocampus. *J Physiol* 493:707–717.
- Avoli M, de Curtis M, Gnatkovsky V, Gotman J, Köhling R, Lévesque M, Manseau F, Shiri Z, Williams S (2016) Specific imbalance of excitatory/inhibitory signaling establishes seizure onset pattern in temporal lobe epilepsy. *J Neurophysiol* 115:3229–3237.
- Bean BP (2007) The action potential in mammalian central neurons. *Nat Rev Neurosci* 8:451–465.
- Beed P, Gundlfinger A, Schneiderbauer S, Song J, Böhm C, Burgalossi A, Brecht M, Vida I, Schmitz D (2013) Inhibitory gradient along the dorsoventral axis in the medial entorhinal cortex. *Neuron* 79:1197–1207.
- Behr C, D'Antuono M, Hamidi S, Herrington R, Lévesque M, Salami P, Shiri Z, Köhling R, Avoli M (2014) Limbic networks and epileptiform synchronization: the view from the experimental side. *Int Rev Neurobiol* 114:63–87.
- Boido D, Jesuthasan N, de Curtis M, Uva L (2014a) Network dynamics during the progression of seizure-like events in the hippocampal-parahippocampal regions. *Cereb Cortex* 24:163–173.
- Boido D, Gnatkovsky V, Uva L, Francione S, de Curtis M (2014b) Simultaneous enhancement of excitation and postburst inhibition at the end of focal seizures. *Ann Neurol* 76:826–836.
- Bragin A, Engel J, Wilson CL, Vizin E, Mathern GW (1999) Electrophysiologic analysis of a chronic seizure model after unilateral hippocampal KA injection. *Epilepsia* 40:1210–1221.
- Cammarota M, Losi G, Chiavegato A, Zonta M, Carmignoto G (2013) Fast spiking interneuron control of seizure propagation in a cortical slice model of focal epilepsy. *J Physiol* 591:807–822.
- Cardin JA, Carlén M, Meletis K, Knoblich U, Zhang F, Deisseroth K, Tsai LH, Moore CI (2009) Driving fast-spiking cells induces gamma rhythm and controls sensory responses. *Nature* 459:663–667.
- Chang M, Dian JA, Dufour S, Wang L, Moradi Chameh H, Ramani M, Zhang L, Carlen PL, Womelsdorf T, Valiante TA (2018) Brief activation of GABAergic interneurons initiates the transition to ictal events through post-inhibitory rebound excitation. *Neurobiol Dis* 109:102–116.
- Chever O, Zerimech S, Scalmani P, Lemaire L, Pizzamiglio L, Loucif A, Ayrault M, Krupa M, Desroches M, Duprat F, Léna I, Cestèle S, Mantegazza M (2021) Initiation of migraine-related cortical spreading depolarization by hyperactivity of GABAergic neurons and NaV1.1 channels. *J Clin Invest* 131:e142203.
- Chiang CC, Ladas TP, Gonzalez-Reyes LE, Durand DM (2014) Seizure suppression by high frequency optogenetic stimulation using *in vitro* and *in vivo* animal models of epilepsy. *Brain Stimul* 7:890–899.
- Codadu NK, Graham RT, Burman RJ, Jackson-Taylor RT, Raimondo JV, Trevelyan AJ, Parrish RR (2019) Divergent paths to seizure-like events. *Physiol Rep* 7:e14226.
- Couey JJ, Witoelar A, Zhang SJ, Zheng K, Ye J, Dunn B, Czajkowski R, Moser MB, Moser EI, Roudi Y, Witter MP (2013) Recurrent inhibitory circuitry as a mechanism for grid formation. *Nat Neurosci* 16:318–324.
- de Curtis M, Avoli M (2016) GABAergic networks jump-start focal seizures. *Epilepsia* 57:679–687.
- Derchansky M, Jahromi SS, Mamani M, Shin DS, Sik A, Carlen PL (2008) Transition to seizures in the isolated immature mouse hippocampus: a switch from dominant phasic inhibition to dominant phasic excitation. *J Physiol* 586:477–494.
- Devinsky O, Vezzani A, O'Brien TJ, Jette N, Scheffer IE, de Curtis M, Perucca P (2018) Epilepsy. *Nat Rev Dis Prim* 4:18024.
- Di Cristo G, Awad PN, Hamidi S, Avoli M (2018) KCC2, epileptiform synchronization, and epileptic disorders. *Prog Neurobiol* 162:1–16.
- Di Giacomo R, Uribe-San-Martin R, Mai R, Francione S, Nobili L, Sartori I, Gozzo F, Pelliccia V, Onofrij M, Lo Russo G, de Curtis M, Tassi L (2019) Stereo-EEG ictal/interictal patterns and underlying pathologies. *Seizure* 72:54–60.
- Dzhala VI, Staley KJ (2003) Excitatory actions of endogenously released GABA contribute to initiation of ictal epileptiform activity in the developing hippocampus. *J Neurosci* 23:1840–1846.
- Elahian B, Lado NE, Mankin E, Vangala S, Misra A, Moxon K, Fried I, Sharan A, Yeasin M, Staba R, Bragin A, Avoli M, Sperling MR, Engel J, Weiss SA (2018) Low-voltage fast seizures in humans begin with increased interneuron firing. *Ann Neurol* 84:588–600.
- Engel J (1990) The Hans Berger lecture. Functional explorations of the human epileptic brain and their therapeutic implications. *Electroencephalogr Clin Neurophysiol* 76:296–316.
- Fernandez FR, Via G, Canavier CC, White JA (2022) Kinetics and connectivity properties of parvalbumin- and somatostatin-positive inhibition in layer 2/3 medial entorhinal cortex. *eNeuro* 9:ENEURO.0441-21.2022.
- Ferrante M, Tahvildari B, Duque A, Hadzipasic M, Salkoff D, Zaghera EW, Hasselmo ME, McCormick DA (2017) Distinct functional groups emerge from the IntrNLic properties of molecularly identified entorhinal interneurons and principal cells. *Cereb Cortex* 27:3186–3207.
- Freund TF, Buzsáki G (1996) Interneurons of the hippocampus. *Hippocampus* 6:347–470.
- Fuchs EC, Neitz A, Pinna R, Melzer S, Caputi A, Monyer H (2016) Local and distant input controlling excitation in layer II of the medial entorhinal cortex. *Neuron* 89:194–208.
- Fujita S, Toyoda I, Thamattoor AK, Buckmaster PS (2014) Preictal activity of subicular, CA1, and dentate gyrus principal neurons in the dorsal hippocampus before spontaneous seizures in a rat model of temporal lobe epilepsy. *J Neurosci* 34:16671–16687.
- Fujiwara-Tsukamoto Y, Isomura Y, Imanishi M, Fukai T, Takada M (2007) Distinct types of ionic modulation of GABA actions in pyramidal cells and interneurons during electrical induction of hippocampal seizure-like network activity. *Eur J Neurosci* 25:2713–2725.
- Gallopin T, Geoffroy H, Rossier J, Lambolez B (2006) Cortical sources of CRF, NKB, and CCK and their effects on pyramidal cells in the neocortex. *Cereb Cortex* 16:1440–1452.
- Gnatkovsky V, Librizzi L, Trombin F, de Curtis M (2008) Fast activity at seizure onset is mediated by inhibitory circuits in the entorhinal cortex *in vitro*. *Ann Neurol* 64:674–686.
- Gnatkovsky V, Pelliccia V, de Curtis M, Tassi L (2019) Two main focal seizure patterns revealed by intracerebral electroencephalographic biomarker analysis. *Epilepsia* 60:96–106.
- Goff KM, Goldberg EM (2019) Vasoactive intestinal peptide-expressing interneurons are impaired in a mouse model of Dravet syndrome. *Elife* 8:e46846.
- Goldberg EM, Clark BD, Zaghera E, Nahmani M, Erisir A, Rudy B (2008) K⁺ channels at the axon initial segment dampen near-threshold excitability of neocortical fast-spiking GABAergic interneurons. *Neuron* 58:387–400.
- Grasse DW, Karunakaran S, Moxon KA (2013) Neuronal synchrony and the transition to spontaneous seizures. *Exp Neurol* 248:72–84.
- Helm J, Akgul G, Wollmuth LP (2013) Subgroups of parvalbumin-expressing interneurons in layers 2/3 of the visual cortex. *J Neurophysiol* 109:1600–1613.

- Hjorth J, Blackwell KT, Kotaleski JH (2009) Gap junctions between striatal fast-spiking interneurons regulate spiking activity and synchronization as a function of cortical activity. *J Neurosci* 29:5276–5286.
- Jenerick H (1963) Phase plane trajectories of the muscle spike potential. *Biophys J* 3:363–377.
- Kaila K, Lamsa K, Smirnov S, Taira T, Voipio J (1997) Long-lasting GABA-mediated depolarization evoked by high-frequency stimulation in pyramidal neurons of rat hippocampal slice is attributable to a network-driven, bicarbonate-dependent K⁺ transient. *J Neurosci* 17:7662–7672.
- Kaila K, Ruusuvaara E, Seja P, Voipio J, Puskarjov M (2014) GABA actions and ionic plasticity in epilepsy. *Curr Opin Neurobiol* 26:34–41.
- Karson MA, Tang AH, Milner TA, Alger BE (2009) Synaptic cross talk between perisomatic-targeting interneuron classes expressing cholecystokinin and parvalbumin in hippocampus. *J Neurosci* 29:4140–4154.
- Kawaguchi Y, Kondo S (2002) Parvalbumin, somatostatin and cholecystokinin as chemical markers for specific GABAergic interneuron types in the rat frontal cortex. *J Neurocytol* 31:277–287.
- Kecskés M, Henn-Mike N, Agócs-Laboda Á, Szócs S, Petykó Z, Varga C (2020) Somatostatin expressing GABAergic interneurons in the medial entorhinal cortex preferentially inhibit layer III-V pyramidal cells. *Commun Biol* 3.
- Klausberger T, Marton LF, O’Neill J, Huck JHJ, Dalezios Y, Fuentealba P, Suen WY, Papp E, Kaneko T, Watanabe M, Csicsvari J, Somogyi P (2005) Complementary roles of cholecystokinin- and parvalbumin-expressing GABAergic neurons in hippocampal network oscillations. *J Neurosci* 25:9782–9793.
- Köhling R, D’Antuono M, Benini R, de Guzman P, Avoli M (2016) Hypersynchronous ictal onset in the perirhinal cortex results from dynamic weakening in inhibition. *Neurobiol Dis* 87:1–10.
- Lado WE, Xu X, Hablitz JJ (2022) Modulation of epileptiform activity by three subgroups of GABAergic interneurons in mouse somatosensory cortex. *Epilepsy Res* 183:106937.
- Lagarde S, Bonini F, McGonigal A, Chauvel P, Gavaret M, Scavarda D, Carron R, Régis J, Aubert S, Villeneuve N, Giusiano B, Figarella-Branger D, Trebuchon A, Bartolomei F (2016) Seizure-onset patterns in focal cortical dysplasia and neurodevelopmental tumors: relationship with surgical prognosis and neuropathologic subtypes. *Epilepsia* 57:1426–1435.
- Laszóczi B, Nyitrai G, Héja L, Kardos J (2009) Synchronization of GABAergic inputs to CA3 pyramidal cells precedes seizure-like event onset in juvenile rat hippocampal slices. *J Neurophysiol* 102:2538–2553.
- Lemaire L, Desroches M, Krupa M, Pizzamiglio L, Scalmani P, Mantegazza M (2021) Modeling NaV1.1/SCN1A sodium channel mutations in a microcircuit with realistic ion concentration dynamics suggests differential GABAergic mechanisms leading to hyperexcitability in epilepsy and hemiplegic migraine. *PLoS Comput Biol* 17:e1009239.
- Lévesque M, Salami P, Gotman J, Avoli M (2012) Two seizure-onset types reveal specific patterns of high-frequency oscillations in a model of temporal lobe epilepsy. *J Neurosci* 32:13264–13272.
- Lévesque M, Salami P, Behr C, Avoli M (2013) Temporal lobe epileptiform activity following systemic administration of 4-aminopyridine in rats. *Epilepsia* 54:596–604.
- Lévesque M, Chen LY, Hamidi S, Avoli M (2018) Dynamic interneuron-principal cell interplay leads to a specific pattern of *in vitro* ictogenesis. *Neurobiol Dis* 115:92–100.
- Librizzi L, Losi G, Marcon I, Sessolo M, Scalmani P, Carmignoto G, de Curtis M (2017) Interneuronal network activity at the onset of seizure-like events in entorhinal cortex slices. *J Neurosci* 37:10398–10407.
- Lopantsev V, Avoli M (1998a) Participation of GABA-mediated inhibition in ictal-like discharges in the rat entorhinal cortex. *J Neurophysiol* 79:352–360.
- Lopantsev V, Avoli M (1998b) Laminar organization of epileptiform discharges in the rat entorhinal cortex *in vitro*. *J Physiol* 509:785–796.
- López-Bendito G, Sturgess K, Erdélyi F, Szabó G, Molnár Z, Paulsen O (2004) Preferential origin and layer destination of GAD65-GFP cortical interneurons. *Cereb Cortex* 14:1122–1133.
- Losi G, Cammarota M, Chiavagato A, Gomez-Gonzalo M, Carmignoto G (2010) A new experimental model of focal seizures in the entorhinal cortex. *Epilepsia* 51:1493–1502.
- Mantegazza M, Franceschetti S, Avanzini G (1998) Anemone toxin (ATX II)-induced increase in persistent sodium current: effects on the firing properties of rat neocortical pyramidal neurons. *J Physiol* 507:105–116.
- Merricks EM, Smith EH, Emerson RG, Bateman LM, McKhann GM, Goodman RR, Sheth SA, Greger B, House PA, Trevelyan AJ, Schevon CA (2021) Neuronal firing and waveform alterations through ictal recruitment in humans. *J Neurosci* 41:766–779.
- Miri ML, Vinck M, Pant R, Cardin JA (2018) Altered hippocampal interneuron activity precedes ictal onset. *Elife* 7:e40750.
- Mitterdorfer J, Bean BP (2002) Potassium currents during the action potential of hippocampal CA3 neurons. *J Neurosci* 22:10106–10115.
- Miyamae T, Chen K, Lewis DA, Gonzalez-Burgos G (2017) Distinct physiological maturation of parvalbumin-positive neuron subtypes in mouse prefrontal cortex. *J Neurosci* 37:4883–4902.
- Neske GT, Patrick SL, Connors BW (2015) Contributions of diverse excitatory and inhibitory neurons to recurrent network activity in cerebral cortex. *J Neurosci* 35:1089–1105.
- Nguyen R, Venkatesan S, Binko M, Bang JY, Cajanding JD, Briggs C, Sargin D, Imayoshi I, Lambe EK, Kim JC (2020) Cholecystokinin-expressing interneurons of the medial prefrontal cortex mediate working memory retrieval. *J Neurosci* 40:2314–2331.
- Ogren JA, Bragin A, Wilson CL, Hoftman GD, Lin JJ, Dutton RA, Fields TA, Toga AW, Thompson PM, Engel J Jr, Staba RJ (2009) Three-dimensional hippocampal atrophy maps distinguish two common temporal lobe seizure-onset patterns. *Epilepsia* 50:1361–1370.
- Pelkey KA, Chittajallu R, Craig MT, Tricoire L, Wester JC, McBain CJ (2017) Hippocampal GABAergic inhibitory interneurons. *Physiol Rev* 97:1619–1747.
- Velazquez JL, Carlen PL (1999) Synchronization of GABAergic interneuronal networks during seizure-like activity in the rat horizontal hippocampal slice. *Eur J Neurosci* 11:4110–4118.
- Perucca P, O’Brien TJ (2015) Epilepsy in 2014. Novel and large collaborations drive advances in epilepsy. *Nat Rev Neurol* 11:74–76.
- Pfeffer CK, Xue M, He M, Huang ZJ, Scanziani M (2013) Inhibition of inhibition in visual cortex: the logic of connections between molecularly distinct interneurons. *Nat Neurosci* 16:1068–1076.
- Riban V, Boullier V, Pham-Lê BT, Fritschy JM, Marescaux C, Depaulis A (2002) Evolution of hippocampal epileptic activity during the development of hippocampal sclerosis in a mouse model of temporal lobe epilepsy. *Neuroscience* 112:101–111.
- Rudy B, Fishell G, Lee SH, Hjerling-Leffler J (2011) Three groups of interneurons account for nearly 100% of neocortical GABAergic neurons. *Dev Neurobiol* 71:45–61.
- Salami P, Lévesque M, Gotman J, Avoli M (2015) Distinct EEG seizure patterns reflect different seizure generation mechanisms. *J Neurophysiol* 113:2840–2844.
- Shiri Z, Manseau F, Lévesque M, Williams S, Avoli M (2015) Interneuron activity leads to initiation of low-voltage fast-onset seizures. *Ann Neurol* 77:541–546.
- Shiri Z, Manseau F, Lévesque M, Williams S, Avoli M (2016) Activation of specific neuronal networks leads to different seizure onset types. *Ann Neurol* 79:354–365.
- Singh S, Sandy S, Wiebe S (2015) Ictal onset on intracranial EEG: do we know it when we see it? State of the evidence. *Epilepsia* 56:1629–1638.
- Tamamaki N, Yanagawa Y, Tomioka R, Miyazaki JI, Obata K, Kaneko T (2003) Green fluorescent protein expression and colocalization with calretinin, parvalbumin, and somatostatin in the GAD67-GFP knock-in mouse. *J Comp Neurol* 467:60–79.
- Toyoda I, Fujita S, Thamattoor AK, Buckmaster PS (2015) Unit activity of hippocampal interneurons before spontaneous seizures in an animal model of temporal lobe epilepsy. *J Neurosci* 35:6600–6618.
- Tremblay R, Lee S, Rudy B (2016) GABAergic interneurons in the neocortex: from cellular properties to circuits. *Neuron* 91:260–292.
- Tricoire L, Pelkey KA, Erkkila BE, Jeffries BW, Yuan X, McBain CJ (2011) A blueprint for the spatiotemporal origin of mouse hippocampal interneuron diversity. *J Neurosci* 31:10948–10970.
- Trombin F, Gnatkovsky V, de Curtis M (2011) Changes in action potential features during focal seizure discharges in the entorhinal cortex of the *in vitro* isolated guinea pig brain. *J Neurophysiol* 106:1411–1423.
- Truccolo W, Donoghue JA, Hochberg LR, Eskandar EN, Madsen JR, Anderson WS, Brown EN, Halgren E, Cash SS (2011) Single-neuron dynamics in human focal epilepsy. *Nat Neurosci* 14:635–641.
- Urban-Ciecko J, Barth AL (2016) Somatostatin-expressing neurons in cortical networks. *Nat Rev Neurosci* 17:401–409.
- Uva L, Librizzi L, Wendling F, de Curtis M (2005) Propagation dynamics of epileptiform activity acutely induced by bicuculline in the hippocampal-

- parahippocampal region of the isolated Guinea pig brain. *Epilepsia* 46:1914–1925.
- Uva L, Avoli M, de Curtis M (2009) Synchronous GABA-receptor-dependent potentials in limbic areas of the *in-vitro* isolated adult guinea pig brain. *Eur J Neurosci* 29:911–920.
- Uva L, Trombin F, Carriero G, Avoli M, de Curtis M (2013) Seizure-like discharges induced by 4-aminopyridine in the olfactory system of the *in vitro* isolated guinea pig brain. *Epilepsia* 54:605–615.
- Uva L, Breschi GL, Gnatkovsky V, Taverna S, de Curtis M (2015) Synchronous inhibitory potentials precede seizure-like events in acute models of focal limbic seizures. *J Neurosci* 35:3048–3055.
- Uva L, Boido D, Avoli M, de Curtis M, Lévesque M (2017a) High-frequency oscillations and seizure-like discharges in the entorhinal cortex of the *in vitro* isolated guinea pig brain. *Epilepsy Res* 130:21–26.
- Uva L, Saccucci S, Chikhladze M, Tassi L, Gnatkovsky V, Milesi G, Morbin M, de Curtis M (2017b) A novel focal seizure pattern generated in superficial layers of the olfactory cortex. *J Neurosci* 37:3544–3554.
- Uva L, Aracri P, Forcaia G, de Curtis M (2021) Mapping region-specific seizure-like patterns in the *in vitro* isolated guinea pig brain. *Exp Neurol* 342:113727.
- Varga C, Lee SY, Soltesz I (2010) Target-selective GABAergic control of entorhinal cortex output. *Nat Neurosci* 13:822–824.
- Weiss SA, Staba R, Bragin A, Moxon K, Sperling M, Avoli M, Engel J (2019) Interneurons and principal cell firing in human limbic areas at focal seizure onset. *Neurobiol Dis* 124:183–188.
- Yekhlief L, Breschi GL, Lagostena L, Russo G, Taverna S (2015) Selective activation of parvalbumin- or somatostatin-expressing interneurons triggers epileptic seizurelike activity in mouse medial entorhinal cortex. *J Neurophysiol* 113:1616–1630.
- Zhang ZJ, Koifman J, Shin DS, Ye H, Florez CM, Zhang L, Valiante TA, Carlen PL (2012) Transition to seizure: ictal discharge is preceded by exhausted presynaptic GABA release in the hippocampal CA3 region. *J Neurosci* 32:2499–2512.
- Zhu Q, Ke W, He Q, Wang X, Zheng R, Li T, Luan G, Long YS, Liao WP, Shu Y (2018) Laminar distribution of neurochemically-identified interneurons and cellular co-expression of molecular markers in epileptic human cortex. *Neurosci Bull* 34:992–1006.
- Ziburkus J, Cressman JR, Barreto E, Schiff SJ (2006) Interneuron and pyramidal cell interplay during *in vitro* seizure-like events. *J Neurophysiol* 95:3948–3954.